

+++++

**Architecture and Geometry of Braided Channel Complex in the
Triassic Wolfville Formation**

Jordan D. Nickerson

Submitted in Partial Fulfillment of the Requirements
for the degree of Bachelor of Science, Honours
Department of Earth Sciences,
Dalhousie University, Halifax, Nova Scotia

March 2010

Abstract

The Wolfville Formation crops out along the shoreline of the Minas Basin of the Bay of Fundy, Nova Scotia. Cambridge Cove contains an exceptionally well preserved outcrop which presents 2D and 3D exposures of the braided channel depositional environment of the Wolfville Formation. These outcrops demonstrate the stratigraphic complexities associated with the depositional environment.

This study aims to: 1) investigate the heterogeneity of a braided channel complex including interconnectivity between channel bodies, as well as baffles and barriers to fluid flow within stratigraphic packages, 2) determine the structural controls on reservoir compartmentalization, including sealing and transmissive faults, and 3) discern the potential of these outcrops as an analogue for other early Mesozoic syn-rift and post-rift reservoirs in the subsurface.

Data from measured sections of the outcrops, LiDAR, high resolution photogrammetry, scintillometer readings (gamma ray) and permeameter measurements have been compiled, analyzed; a depositional model of the study area has been constructed. The model demonstrates how the lateral continuity of the architectural elements preferentially allows fluid flow through the higher permeable lithologies and illustrates constraints on the effective drainage of fluids in this simulated subsurface reservoir.

Key Words: Cambridge Cove, Triassic, braided channel architecture, depositional systems, architecture, reservoir compartmentalization, and fluid flow.

Table of Contents

Abstract	i
Table of Contents	ii
List of Figures	iv
List of Tables	vi
Acknowledgements	vii
1.0 Introduction	1
1.1 Study Area.....	2
1.2 Fundy Tides.....	4
1.3 Thesis Organization.....	5
2.0 Geological Background	6
2.1 Fundy Basin.....	6
2.2 Regional setting.....	10
2.3 Fluvial Depositional Systems.....	11
2.3.1 Alluvial Deposits.....	12
2.3.2 Sediment Transport.....	12
2.3.3 Subdivisions of Alluvial Deposits.....	12
2.3.4 Scales of Depositional Units.....	14
2.3.5 Alluvial Facies.....	15
2.3.6 Architectural Elements.....	17
2.3.7 Braid Channel Classification.....	19
3.0 Methods	20
3.1 Measured Sections.....	20
3.2 Gamma Scintillometer.....	21
3.3 Permeameter.....	21
3.4 High Resolution Photography.....	22
3.5 LiDAR.....	23
3.6 Polyworks.....	23
4.0 Results	26
4.1 Outcrop and Measured Section Descriptions.....	26
4.1.1 Lithofacies Descriptions.....	27
Lithofacies 1: Clast-supported Conglomerate.....	27
Lithofacies 2: Matrix-supported Conglomerate.....	28
Lithofacies 3: Sandstone.....	30
Lithofacies 4: Paleosols.....	31
4.1.2 Depositional Cycles.....	32

4.1.3 Section 1.....	3
4.1.4 Section 2.....	3
4.1.5 Section 3.....	3
4.1.6 Section 4.....	3
4.1.7 Section 5.....	4
4.2 Gamma readings.....	4
4.3 Permeability.....	4
4.4 High Resolution Photogrammetry.....	4
4.5 LiDAR.....	4
4.5.1 Section 1.....	4
4.5.2 Section 2.....	4
4.5.3 Section	4
4.5.4 Section 4	5
4.5.5 Faults.....	5
5.0 Depositional Model.....	5
6.0 Discussion.....	5
6.1 Permeability and Fluid Flow.....	5
6.2 Gamma Logs.....	5
6.3 Compartmentalization.....	5
7.0 Conclusions.....	6
8.0 References.....	6

List of Figures

Figure 1.1: Regional setting of study area.....	2
Figure 1.2: Aerial view of the study area.....	3
Figure 1.3: 20m cliff section study area.....	3
Figure 2.1: The Fundy Basin southwest plunging synform.....	7
Figure 2.2: Sediments of the Fundy Basin and other Mesozoic Syn-Rift basins.....	8
Figure 2.3: Stratigraphic framework of the Fundy Basin.....	10
Figure 2.4: Triassic/Carboniferous angular unconformity marked in red, Cambridge Cove..	11
Figure 2.5: Features of two types of fluvial systems.....	13
Figure 2.6: Classification of channel patterns.....	13
Figure 2.7: Architectural elements in large scale fluvial deposits.....	18
Figure 3.1: Permeability calibration chart issued by New England research.....	22
Figure 3.2: Aerial photograph of study area.....	25
Figure 3.3: Pre-edited aerial LiDAR image of study area.....	25
Figure 3.4: Post-edited aerial LiDAR image of study area.....	25
Figure 4.1: Aerial view of the Cambridge Cove study area showing the measured locations	26
Figure 4.2: Clast-supported conglomerate at Cambridge Cove, lithofacies 1.....	28
Figure 4.3: 10 meter barform comprising clastic conglomerate, lithofacies 1.....	28
Figure 4.4: Matrix-supported conglomerate at Cambridge Cove.....	29
Figure 4.5: Low angle cross-bedding in matrix-supported conglomerate, lithofacies 2.....	29
Figure 4.6: Sandstone lithofacies 3 and matrix-supported conglomerate, lithofacies 2.....	30
Figure 4.7: Paleosol (lithofacies 4) horizons.....	31
Figure 4.8: Measured section #1 divided into three depositional cycles.....	33
Figure 4.9: Measured section #1.....	34
Figure 4.10: Measured section #2 divided into three depositional cycles.....	35
Figure 4.11: Measured section #2.....	36
Figure 4.12: Measured section #3 divided into four depositional cycles.....	37
Figure 4.13: Measured section #3.....	38
Figure 4.14: Measured section #4 divided into 5 depositional cycles.....	39
Figure 4.15: Measured section #4.....	40
Figure 4.16: Measured section #5, divided into 4 depositional cycles.....	41
Figure 4.17: Measured section #5.....	42
Figure 4.18: Gamma curve for section #1.....	43
Figure 4.19: Locations of permeability tests on stratigraphic section #2.....	45
Figure 4.20: Aerial view of the Cambridge Cove study area.....	46
Figure 4.21: Composite photopan of section 1 displaying architectural elements.....	47
Figure 4.22: LiDAR image of section 1 used to accurately measure architectural elements..	47

Figure 4.23: Composite photopan of section 2 displaying architectural elements.....	48
Figure 4.24: LiDAR image of section 2 used to accurately measure architectural elements..	48
Figure 4.25: Composite photopan of section 3 displaying architectural elements.....	49
Figure 4.26: LiDAR image of section 3 used to accurately measure architectural elements..	49
Figure 4.27: Composite photopan of section 4 displaying architectural elements.....	50
Figure 4.28: LiDAR image of section 4 used to accurately measure architectural elements..	50
Figure 4.29: Aerial view of the Cambridge Cove study area showing the locations of faults.	51
Figure 4.30: LiDAR image with all major faults (red) and minor faults	52
Figure 5.1: W/T plot for mobile channel belts; braided & low-sinuosity rivers.....	54
Figure 5.2: Depositional model of late Triassic Wolfville Formation.....	55
Figure 6.1: Multistory channel belts infilled by bar deposits and some preserved channels..	59

List of Tables

Table 2.1: Hierarchy of depositional units in alluvial deposits.....	14
Table 2.2: Facies classification.....	15
Table 2.3: Architectural elements in fluvial deposits.....	17
Table 4.1: Permeability values obtained from stratigraphic section 2.....	44
Table 4.2: Architectural elements found in section 1.....	47
Table 4.3: Architectural elements found in section 2.....	48
Table 4.4: Architectural elements found in section 3.....	49
Table 4.5: Architectural elements found in section 4.....	50
Table 4.6: Major fault descriptions.....	51

Acknowledgements

I would first like to thank my supervisor Dr. Grant Wach for his unconditional support, knowledge and his interest in seeing his students succeed. I would also like to thank Hayley Pothier and Adam Fraser for their help acquiring all the necessary field data to make this thesis possible. I would also like to thank Dr. Pat Ryall of Dalhousie University for the Honour's thesis course and his assistance in correcting my thesis. Finally I would like to thank my parents for their support during the writing of this thesis. Without their contributions, this thesis would not be possible.

Additional thanks are extended out to Joe and Twyla Smith of the Minas View Golf Links for allowing the use of their land to perform the study at Cambridge Cove.

Special thanks also go out to several contributors such as Optech Inc. for their help in processing the LiDAR data; Shell Canada, N.S Department of Energy, NRCan, and NSCC grants for equipment.

1.0 INTRODUCTION

The late Triassic Wolfville Formation unconformably overlies tilted Carboniferous deposits and crops out along the shoreline of the Minas Basin of the Bay of Fundy, Nova Scotia. Cambridge Cove contains an exceptionally well preserved outcrop section in 2D and 3D exposures of the braided channel depositional environment of the Wolfville Formation. These outcrops demonstrate the stratigraphic complexities associated with this environment. The aim of this study is to investigate the heterogeneity of a braided channel complex including reservoir baffles, interconnectivity between channel bodies, barriers to fluid flow within stratigraphic packages, and to demonstrate how the study of an outcrop can help understand the subtle changes that occur in subsurface. Several factors causing reservoir compartmentalization will be investigated, including internal fluid flow baffles and barriers, impermeable faults, shale beds, and diagenesis of the reservoir (Wach, 2009).

Subsurface braided channel complexes are known to be excellent hydrocarbon reservoir. Unfortunately, most commercial attempts to produce these reservoirs have encountered unanticipated problems because reservoir architecture is not well understood, and because changes in geological complexity occur at resolutions below the detection limits of most data-logging instruments (Hodgetts et al., 2004). Geological modeling can be used to improve the understanding of the depositional controls on fluid distribution in a subsurface reservoir. Developing a geological model of the depositional environment is one of the components needed to understand geological complexity in the subsurface. We need to understand the continuity of potential reservoirs in the subsurface before any steps can be made to commercially produce a hydrocarbon

reservoir, or inject CO₂ for geological sequestration. Information from the Cambridge Cove study area gathered for the preparation of this thesis can be used as an analogue for similar subsurface reservoirs. Although two different deposits will never be the same in every aspect, they can however contain features that are common to each reservoir.

1.1 Study Area

The Wolfville Formation crops out along the south shore of the Minas Basin of the Bay of Fundy, Nova Scotia. Cambridge Cove is located 80 km north of Halifax and was chosen for this study for the excellent exposures of the Wolfville Formation (Fig. 1.1).

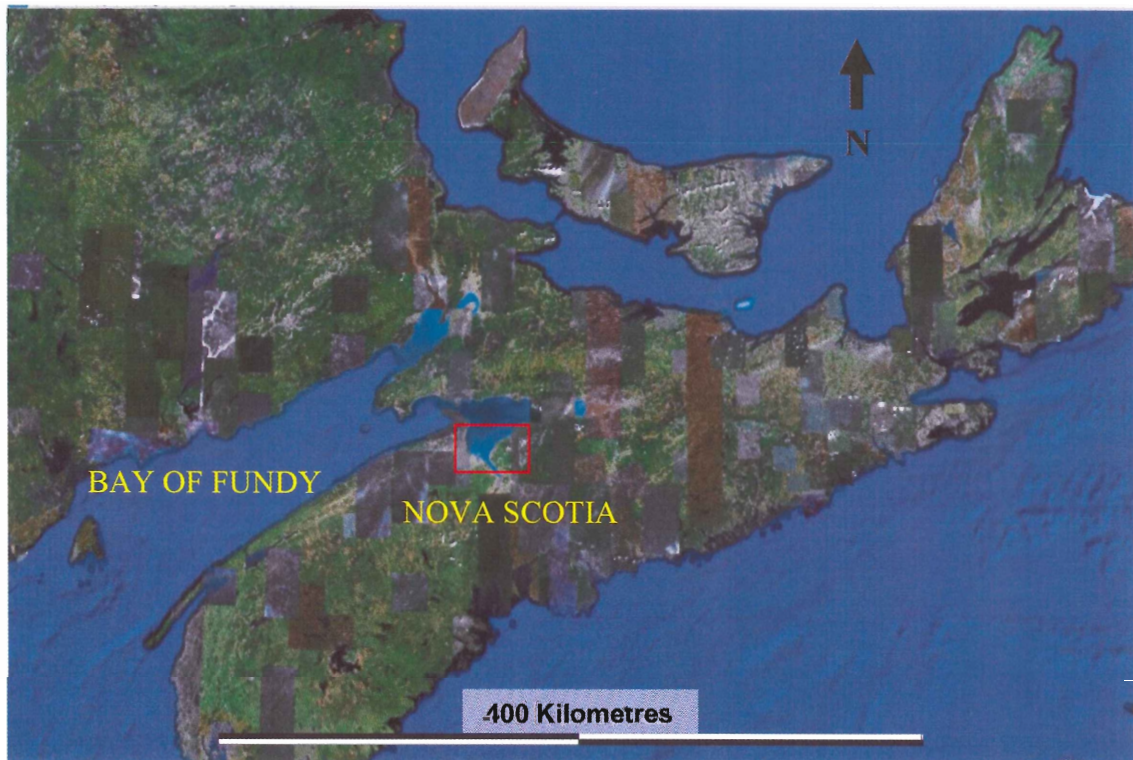


Figure 1.1: Regional setting of study area outlined in red (Google Earth, 2009).

Cambridge Cove is situated near the small community of Cambridge, which is accessed from Hintz Road, near the Minas View Golf Links. a foot trail leads down to the Minas Basin shoreline. A two kilometer hike northeast along the shoreline is required to access the base of a 20m cliff face that is the study area. Figures 1.2 and 1.3 show photographs of the study area and Cambridge Cove access.

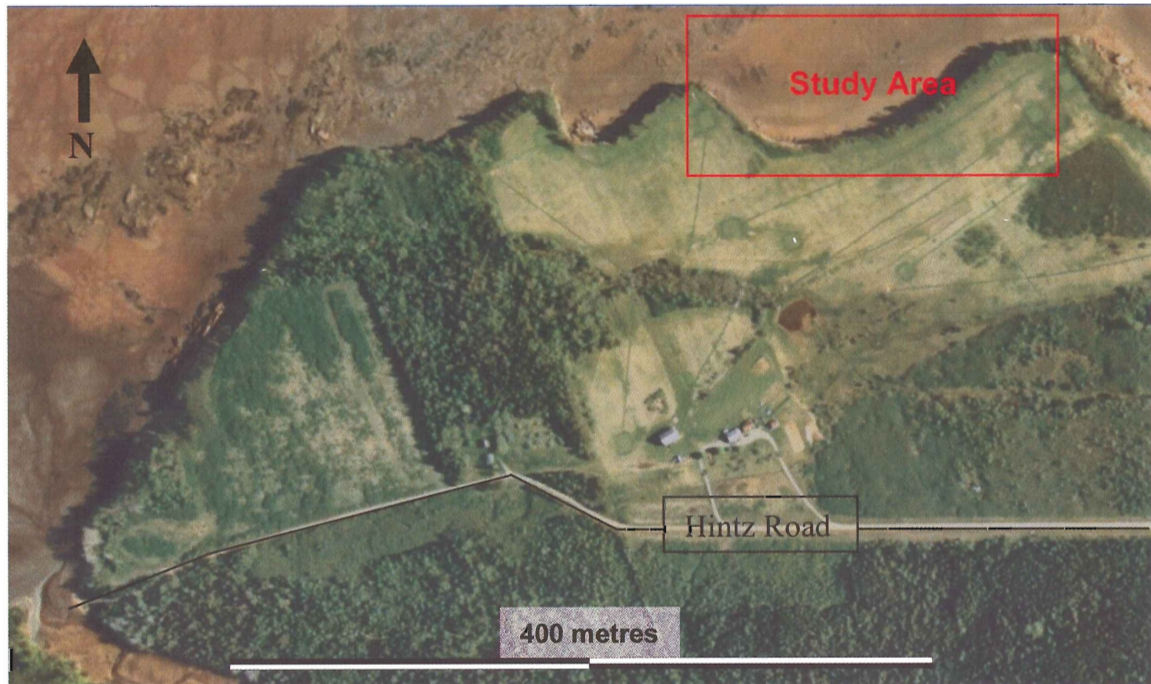


Figure 1.2: Aerial view of the study area (Modified from Monette, 2008).



Figure 1.3: 20 metre cliff section study area.

1.2 Fundy Tides

The Minas Basin is subjected to some of the highest tides in the world. Field work was organized to coincide with tidal fluctuations of approximately 13 m within the area. At high tide, the lower 2 m of the Cambridge Cove cliff section is covered by the waters of the Minas Basin, which consequently does not permit any field work on the cliff face. At low tide the waters of the Minas Basin withdraw far into the Bay of Fundy leaving the study area accessible for field work. A keen eye must be kept on the advancing waters after the tides have ebbed due to the extremely fast-paced influx of sea water back into the Minas Basin. Continuously changing tide times throughout the study season were tracked to optimize data collection and to prevent being trapped along the cliff face by rising waters. The Canadian Hydrographic Service provides tide

tables of the area which helped us plan a safe and productive field work strategy. **1.3**

Thesis Organization

Field work for this thesis was conducted during the 2009 summer season. Analyses, modeling and thesis writing was done during the fall and winter terms of the 2009/10 academic year. This outline shows how this thesis is organized and how the results are displayed.

- Introduction, study area, and thesis organization
- Geological history and literature review
- Methodology
- Field data results
- Depositional modeling
- Discussion
- Conclusions.

2.0 Geological Background

This chapter will discuss the formation of the Fundy Basin and rocks that occupy this basin. The Wolfville Formation is the first of a series of sedimentary and igneous rocks to be deposited within the Fundy Basin. The mode in which the sediments of the Wolfville Formation were deposited will be discussed in detail to establish background knowledge and familiarize the reader with the nomenclature that will be used in this thesis.

2.1 Fundy Basin

The Fundy Basin is one of a series of basins that were formed as a direct result of continental rifting in the Early Mesozoic. As the supercontinent Pangaea started rifting, separating the land mass into Africa and North America, a series of rift valleys formed, extending from Florida to Newfoundland, as a result of these extensional forces (Olsen and Schlische, 1990). The Fundy Basin was created during this orogenic event and is the remnant of the failed attempt to split Africa and North America at that junction. Extensional forces partially separated the continental crust forming a southwest plunging synform (Fig. 2.1). However, rifting shifted to the southeast and crust continued to separate, forming the continents Africa and North America (Wade et al., 1996).

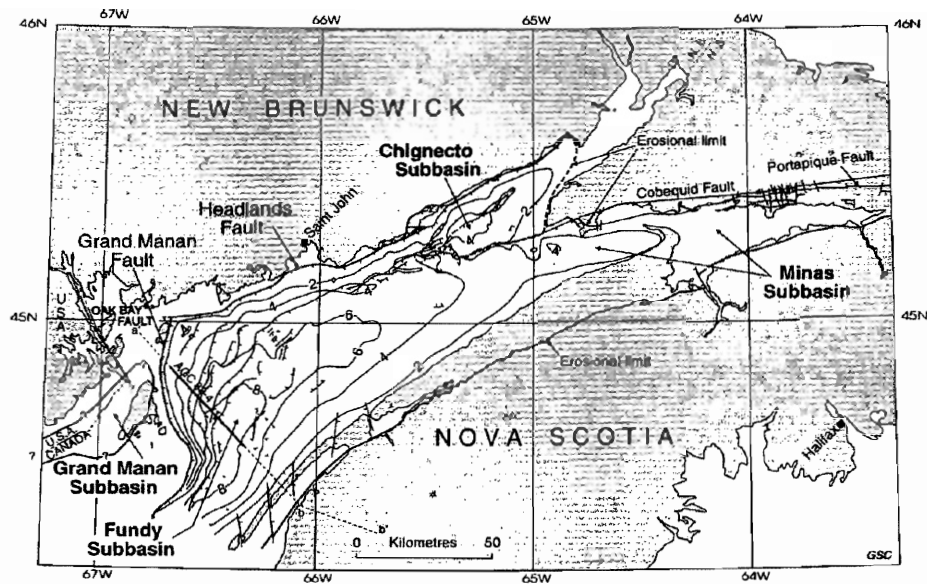


Figure 2.1: The Fundy Basin southwest plunging synform (Wade et al., 1996).

The Fundy Basin is a set of smaller, failed rifted basins that form the main synform structure. The Fundy Basin is comprised of the Chignecto, Fundy, Grand Manan, and the Minas subbasins (Wade et al., 1996). The Minas Fault Zone in the Bay of Fundy was reactivated during the Early Mesozoic which caused left-oblique slip to occur at the same time as the dip-slip deformation driven by extension (Keppie, 1982). Two phases of deformation within the Fundy Basin caused two styles of synrift-sedimentation and deformation to occur within each basin. The Minas subbasin is situated along this east-trending Minas Fault Zone and separates the Avalon Terrane from the Meguma Terrane and underwent left-oblique slip causing the Minas subbasin to extend latterly into the heart of present day Nova Scotia (Keppie, 1982). The Minas Basin contains a large amount of Triassic synrift sediments (Fig. 2.2), which comprise several different lithologies. Most of these sediments have been relatively undisturbed, except for periods of increased sedimentation due to pulses of tectonic activity and igneous flows from sporadic volcanic events (Olsen, 1990).

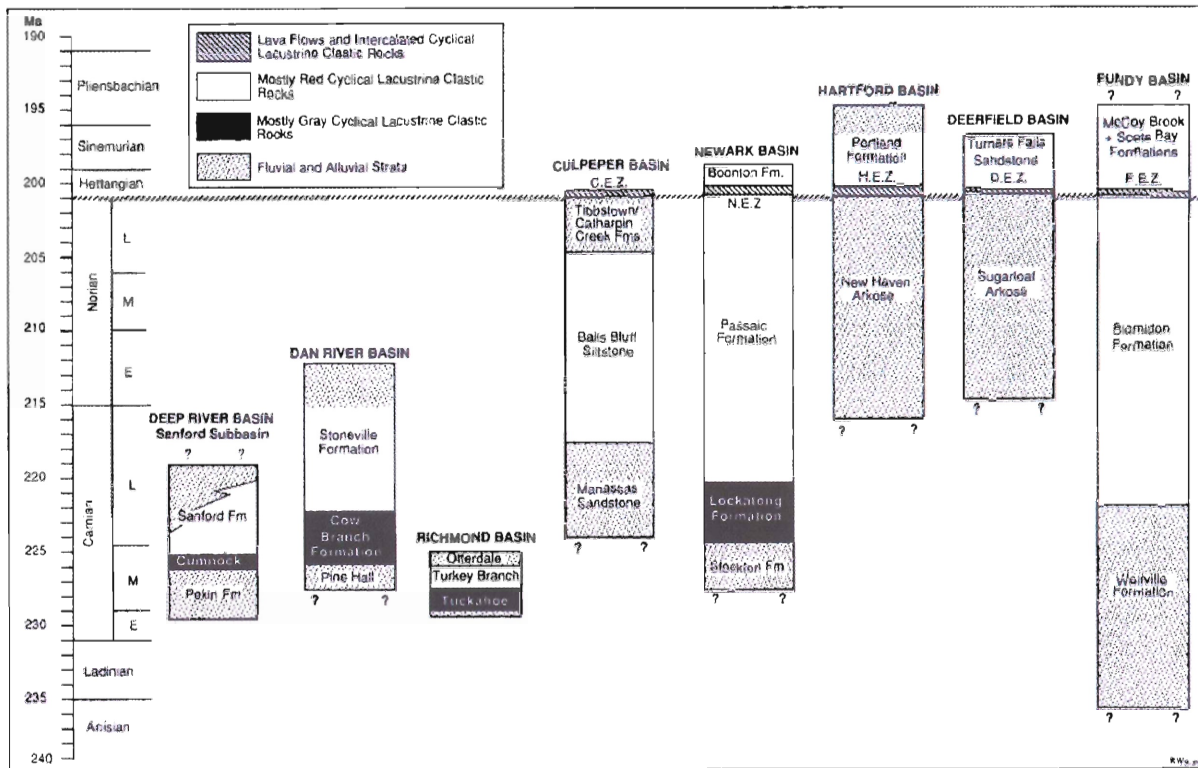


Figure 2.2: Sediments of the Fundy Basin and other Mesozoic synrift basins (Olsen, 1989).

During the Mid-Atlantic rifting event, several basins formed which contain sedimentary and volcanic rocks that are genetically similar to those of the Fundy Rift System and have been named the Newark Supergroup. Figure 2.2 demonstrates the correlation of these lithologies along the basins of the Atlantic seaboard (Olsen, 1990).

The earliest sediment to be deposited in the Fundy Basin is that of the Wolfville Formation. The Wolfville Formation contains fining-upward successions of clast dominant conglomerates, matrix dominated conglomerates and coarse-grained sandstones. The sediment of the Wolfville Formation was deposited from fast-flowing streams and braided rivers sourced from the Meguma Highlands. Rivers flowed from the highlands onto alluvial fans depositing large, spatially continuous, thick successions of poorly sorted conglomerates and sandstones into the depocentres of the Fundy

Basin (Hubert and Forlenza, 1988). Winds reworked the sediments during depositional hiatus, creating thin layers of eolian material, which were further reworked and preserved by subsequent deposition of alluvial sediments (Leleu et al., 2009).

As the climate warmed and became more arid, sediment input into the basin decreased causing evaporites within the inland lake to precipitate and form thick gypsum and mud successions known as the Blomidon Formation (Hubert and Mertz, 1984). Towards the end of the Triassic and into the Jurassic, stresses associated with the final rifting of Pangaea caused volcanic fissures to form and erupt (volcanic) basalt across the entire floor of the Fundy Basin, known as the North Mountain Basalt Formation. The upper formations of the Fundy Group are the Scots Bay and the McCoy Brook Formations, which can be found sporadically distributed within the different subbasins of the Fundy Basin (Hubert and Forlenza, 1988).

Figure 2.3 illustrates the stratigraphic framework of the Fundy Basin. It should be noted that not all of the formations of the Fundy Group are present in each of the subbasins due to depositional hiatus and erosion during the opening of the Fundy Basin and the subsequent development of the Atlantic Ocean during the Cretaceous (Hubert and Forlenza, 1988).

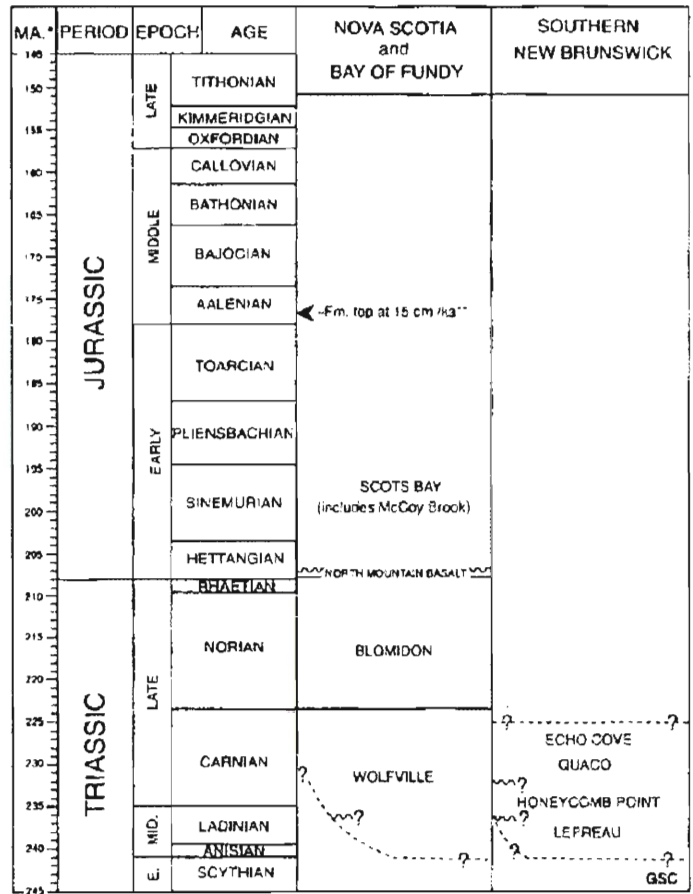


Figure 2.3: Stratigraphic framework of the Fundy Basin (Wade et al., 1996).

2.2 Regional Setting

This study focuses on the lower 50 m of the Wolfville Formation (Fundy Group) which was deposited mainly during the Anisian stage of the Triassic period and consist of fluvial deposited sandstones and conglomerates. The Wolfville Formation crops out laterally along the headlands of the southern shore of the Minas Basin from Cambridge Cove to Burtcoat Head with small interruptions in its continuity. Within the study area of Cambridge Cove, the alternating layers of sandstone and conglomerate of the Wolfville Formation can be found unconformably overlying the Carboniferous rocks of the Horton Group (Fig. 2.4) with a regional dip of about 5° to the NE. These sandstone and

conglomerate beds lie perpendicular to the steeply dipping shale and sandstone beds of the Lower Horton Group, which defines the an angular unconformity. This unconformity represents approximately a 40 million year hiatus due to uplift and erosion of the Carboniferous rocks, followed by subsidence of the Fundy Basin and deposition of the Triassic sediments into the newly formed Fundy Basin (Baird and Olsen, 1983).

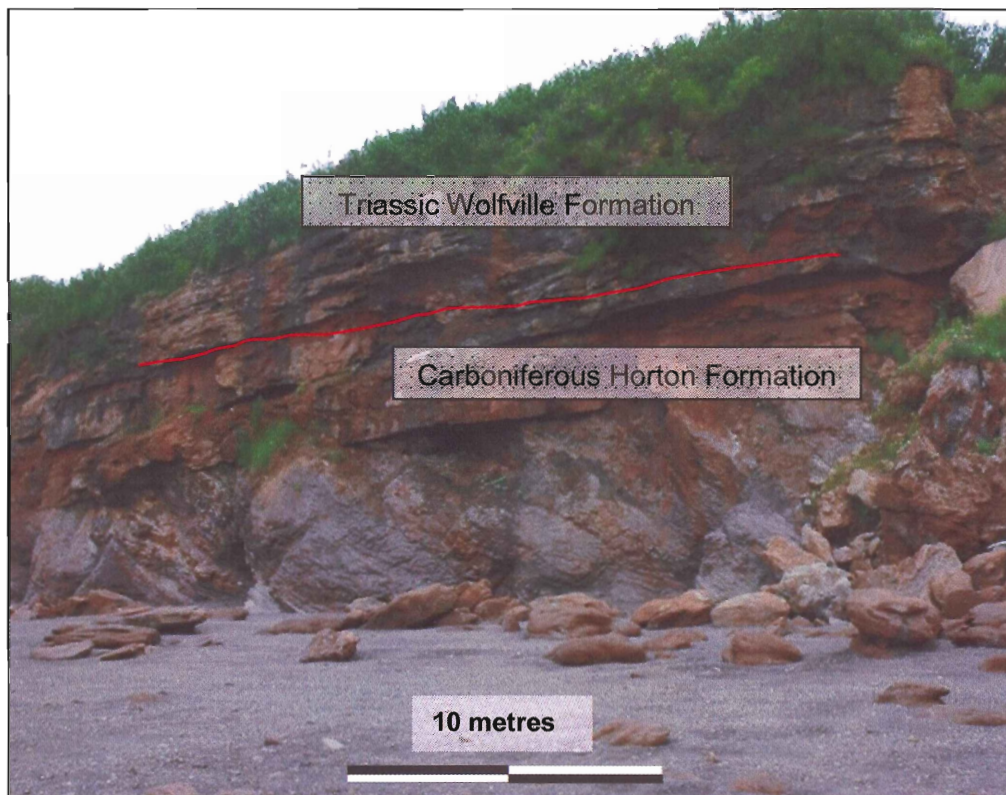


Figure 2.4: Triassic/Carboniferous angular unconformity marked in red, Cambridge Cove.

2.3 Fluvial Depositional Systems

To interpret the past depositional environment of the Wolfville Formation one needs to understand the sedimentary processes from which it was formed. Interpreting depositional history requires investigating the outcrops, or core samples, for sedimentary structures that will aid in determining the depositional process of formation. The strata are classified into lithofacies, which are grouped into environmental facies as the understanding of the sedimentary strata evolves.

2.3.1 Alluvial Deposits

Sediments deposited in an alluvial setting contain a variety of grain sizes ranging from clay- to clast-supported gravel. The process in which the sediment is deposited will dictate the clastic type; slow-moving water along low-relief coastal plains will deposit fine-grained clays and silts, whereas fast-moving water on high-relief slopes will deposit coarse-grained sediments such as gravel (Miall, 1992).

2.3.2 Sediment Transport

Waterborne sediment is transported via two mechanisms: traction currents and sediment gravity flows (Miall, 1992). Traction currents transport unconsolidated sediment, or large clasts, by rolling them via hydraulic forces or temporarily suspending the grains within the water column flow. Larger clasts are deposited in areas of decreased hydraulic force. As a result, bedforms develop. Clastics that are suspended within the water column settle in areas where the current decreases in velocity (Miall, 1992).

2.3.3 Subdivisions of Alluvial Deposits

Miall (1992) describes various types of small-scale stratification and bedforms in alluvial deposits which can help understand depositional processes. Channels and bedforms are formed from several different processes in alluvial deposits. Determining how the structures were formed can be used to describe the depositional environment. Depositional environments can be sub-divided into environmental facies. Bedforms and sedimentary structures is reflected in the architecture and geometry of the stratigraphy. Figure 2.5 illustrates two different alluvial depositional settings and some of the architectural elements.

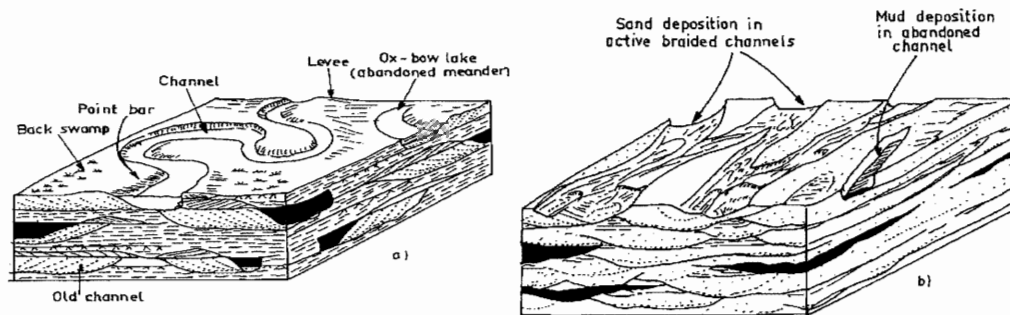


Figure 2.5: Features of two types of fluvial systems. A) meandering B) braided (Miall, 1992).

Fluvial channels are generally subdivided into four categories; meandering, braided, anastomosed and straight. Figure 2.6 from Makaske (1998) illustrates these four types of channel patterns. Defining features of a braid channel complex will be discussed later in this section.

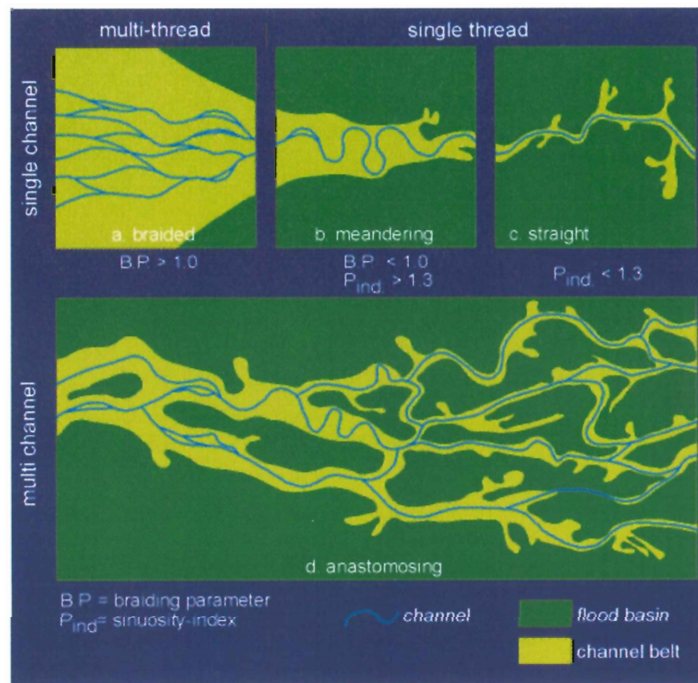


Figure 2.6: Classification of channel patterns (Makaske, 1998).

2.3.4 Scales of Depositional Units

Clastic deposits are described in terms of their natural depositional units, usually described in order of increasing scale; laminae, laminae set, bed, bedset, member, formation, group and basin fill (Campbell 1967; Miall 1991b). The duration of deposition, sediment rate, and the nature of contacts (Campbell, 1967) between the units determines the rank and bounding surface characteristics (Table 2.1). Campbell (1967) emphasized that the contact provided important data on the sedimentary process, whether it was a gradational, a sharp or an erosional surface.

Table 2.1: Hierarchy of depositional units in alluvial deposits (Miall, 1991b).

Group	Time Scale	Example	Sedimentation Rate (m/Ka)	Fluvial depositional units	Rank and characteristics of bounding surfaces
1	10^{-6}	Burst-sweep cycle		Lamina	0th-order, lamination surface
2	10^{-5} - 10^{-4}	Bedform migration	10^5	Ripple (microform)	1st-order, set bounding surface
3	10^{-3}	Bedform migration	10^5	Diurnal dune increment, reactivation surface	1st-order, set bounding surface
4	10^{-2} - 10^{-1}	Bedform migration	10^4	Dune (mesoform)	2nd-order, coset bounding surfaces
5	10^0 - 10^1	Seasonal events	10^2 - 10^3	Macroform growth increment	3rd-order, slipping 5-20° in direction of accretion
6	10^2 - 10^3	100-year flood	10^2 - 10^3	Macroform, e.g. point bar, levee, splay	4th-order, convex-up macroform top
7	10^3 - 10^4	Long term geomorphic processes	10^0 - 10^1	Channel, Delta lobe	5th-order, flat to concave-up channel base
8	10^4 - 10^5	5th order (Milankovitch) cycles	10^{-1}	Channel belt sequence	6th-order, flat, regionally extensive
9	10^5 - 10^6	4th order (Milankovitch) cycles	10^{-1} - 10^{-2}	Depositional system alluvial fan, sequence	7th-order, sequence boundary; flat, regionally extensive
10	10^6 - 10^7	3rd order cycles, tectonic and eustatic processes	10^{-1} - 10^{-2}	Basin-fill complex	8th-order, regional disconformity

2.3.5 Alluvial Facies

The work conducted at Cambridge Cove involved studying several different lithologies and their associated structures to determine the manner in which they were deposited. A simple classification scheme was suggested by Miall (1978) in which sedimentary structures are associated with the probable depositional sequence and environmental setting. Lithology and sediment origin defines a facies. Miall's classification scheme is illustrated in Table 2.2.

Facies code	Facies	Sedimentary structures	interpretation
--------------------	---------------	-------------------------------	-----------------------

Gms	Massive, matrix supported	Grading	Debris flow
Gm	Massive or crudely bedded gravel	Horizontal bedding, imbrication	Longitudinal bars, lag deposits
Gt	Gravel, stratified	Trough cross beds	Minor channel fills
Gp	Gravel, stratified	Planar cross beds	Longitudinal bars, deltaic growths from older bar remnants
St	Sand, medium to very coarse, may be pebbly	Solitary or grouped trough cross beds	Dunes (lower flow regime)
Sp	Sand, medium to very coarse, may be pebbly	Solitary or grouped planar cross beds	Linguoid, transverse bars, sand waves (lower flow regime)
Sr	Sand, very fine to coarse	Ripple cross lamination	Ripples (lower flow regime)
Sh	Sand, very fine to very coarse, may be pebbly	Horizontal lamination	Planar bed flow (upper flow regime)
Sl	Sand, very fine to very coarse, may be pebbly	Low angle cross beds	Scour fills, washed-out dunes, antidunes
Se	Erosional scours with intraclast	Crude cross bedding	Scour fills
Ss	Sand, fine to very coarse, may be pebbly	Broad, shallow scours	Scour fills
Fl	Sand, silt, mud deposits	Fine lamination, very small ripples	Overbank or waning flood
Fsc	Silt, mud	Laminated to massive	Back swamp deposits
Fm	Mud, silt	Massive, desiccation cracks	Overbank or drape deposits
C	Coal, carbonaceous mud	Plant, mud films	Swamp deposits
P	Carbonate	Pedogenic features	Paleosol

Table 2.2: Facies classification (Miall, 1978).

2.3.6 Architectural Elements

Channel fill and barforms are sedimentary features of fluvial processes, and contain structures that are directly related to environmental faces. Table 2.3, modified from Miall 1985, groups these fluvial structures into eight basic elements and describes associated facies assemblages, architectural elements, and geometry found within each structure.

Element	symbol	Principal facies assemblage	Geometry and relationship
Channels	CH	Any combination	Finger, lens or sheet; concave-up erosional base; scale and shape highly variable; internal concave-up 3rd-order erosion surfaces common
Gravel bars and bedforms	GB	Gm, Gp, Gt	Lens, blanket; usually tabular bodies; commonly interbedded with SB
Sandy bedforms	SB	St, Sp, Sh, Sl, Sr, Se, Ss	Lens, sheet, blanket, wedge, occurs as channel-fills, crevasse splays, minor bars
Downstream-accretion macroforms	DA	St, Sp, Sh, Sl, Sr, Se, Ss	Lens resting on flat or channelled base, with convex-up 3rd-order internal erosion surfaces and upper 4th-order bounding surfaces
Lateral-accretion macroforms	LA	St, Sp, Sh, Sl, Se, Ss, less commonly Gm, Gt	Wedge, sheet, lobe; characterized by internal lateral-accretion 3rd-order surfaces
Sediment gravity flows	SG	Gm, Gms	Lobe, sheet, typically interbedded with GB
Laminated sand sheets	LS	Sh, Sl; Minor Sp, Sr	Sheet, blanket
Overbank fines	OF	Fm, Fl	Thin to thick blankets; commonly interbedded with SB; may fill abandoned channels

Table 2.3: Architectural elements in fluvial deposits (Miall, 1985).

Figure 2.7 illustrates eight basic architectural elements that are found in large-scale fluvial deposits. To the right of each sketch is a symbol in which each element is defined and referenced to Table 2.3. To the left of each sketch is a symbol that defines the associated facies found in each structure and a description of each symbol can be referenced in Table 2.2.

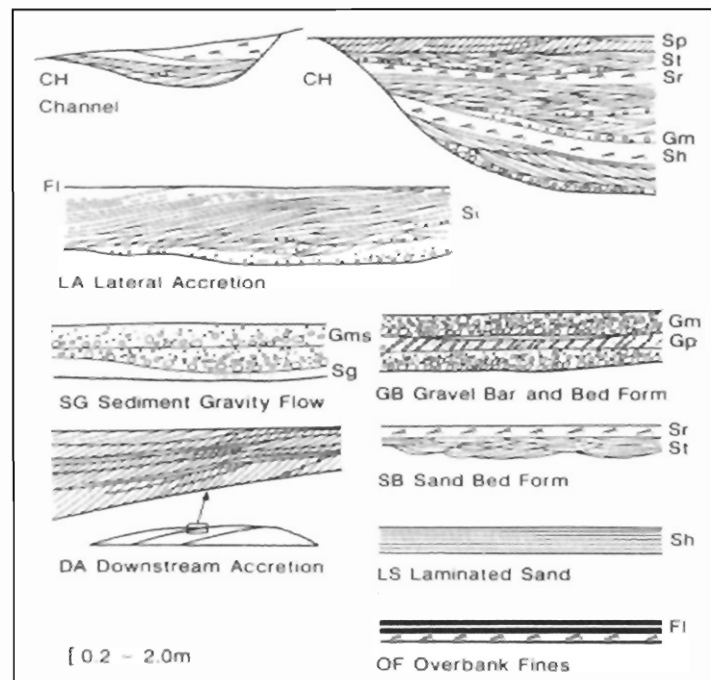


Figure 2.7: Architectural elements in large-scale fluvial deposits (Miall, 1985).

2.3.7 Braid Channel classification.

Alluvial deposits cover a broad range of depositional environments from flood plain sediments to large-scale debris flows (Miall,1985). Although the internal structures of sedimentary beds are important for modeling depositional environments, a more direct approach to determining depositional environment is investigating the magnitude of the physical sedimentary structures that have been produced (Gibling, 2006).

Braided channel deposits are often defined by a diverse group of sandstone and gravel-based deposits found within river systems that can span tens of kilometres in width. Sedimentary structures include bar form deposits and channel bodies that are both horizontally and vertically stacked to form composite deposits. A defining feature of braid-channel deposits is the multi-stacking patterns of channel bodies that have been deposited within erosional features as river channels migrate laterally into the adjacent bar form deposits. This process results in the deposition of vertical and horizontal stacked bar deposits and bed load sheets (Gibling 2006).

3.0 Methods

Field work at the Cambridge Cove study area involved the use of several different sampling methods and techniques to provide the stratigraphic data for this project. The integration of the data into a geological model provides a relatively detailed understanding of the shallow subsurface in the study area.

3.1 Measured Sections

The study area at Cambridge Cove is bounded by 20 m vertical cliff faces which rendered 90% of the outcrop inaccessible to normal methods of acquiring stratigraphic information. It was decided that the use of rock-climbing techniques would allow for the collection of full stratigraphic sections, which would improve the accuracy of the study. Rappelling gear was purchased and rock-climbing training was conducted at Dalhousie's Dalplex to ensure safety while collecting data in the field. Ben Smith, a rock climbing expert from Dalhousie's Dalplex, was hired to supervise the collection of field data and to ensure the proper installation of the rock-climbing equipment.

Five sections were chosen to measurement of complete stratigraphic sections. Locations were chosen to maximize the coverage across the 400 m cliff face. While rappelling down each section sedimentary structures, lithologies, grain and clast sizes, clast lithologies, thicknesses, and structural features were investigated and recorded.

The total thickness of the sections was recorded via tape measure draped over the cliff

face.3.2 Gamma Scintillometer

During the collection of one of the measured sections down the cliff sections, a gamma scintillometer was strapped to the rock climbing gear and a gamma log was

recorded down the cliff face at .5 m intervals. A scintillometer is an instrument used to detect and record gamma radiation from materials that contain elements uranium, thorium and potassium. The gamma rays are detected when they encounter the sodium iodide crystal within the instrument and this results in free electrons and light emissions which are converted into electrical pulses. The stronger the rays encountered, a larger amount of electrical pulses are produced within the instrument. The number of pulses or counts is related to the quantity of radioactive material in the sample (O'Reilly, 1982).

3.3 Permeameter

Permeability values were collected during a descent down one of the measured cliff sections. Values were collected at 3 intervals (Fig. 4.19) using a handheld permeameter, Tiny Perm II, developed by New England Research. The permeameter consists of an air piston that is attached to a handheld computer which displays the results. Permeability values are calculated by engaging the air piston against the rock face and a vacuum is generated from the expulsion of air from the piston. The rate at which air travels through the sample rock into the piston until the pressure equilibrates is output to the handheld computer. Values are displayed on the handheld computer and permeability values are calculated by using a calibration chart provided by New England Research. A copy of the calibration curve is displayed in Figure 3.1.

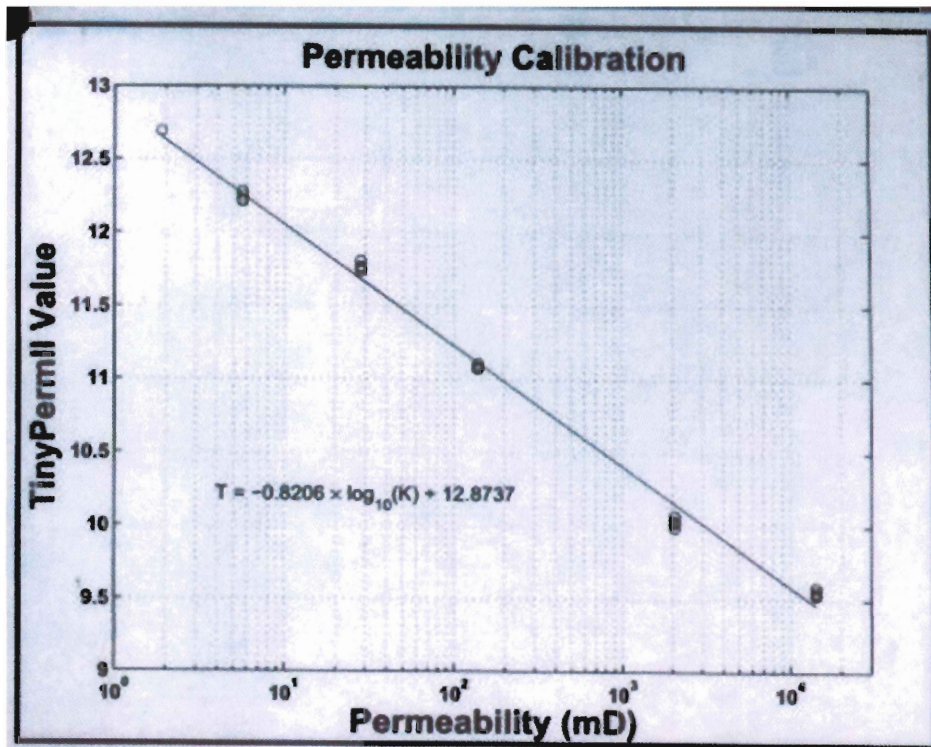


Figure 3.1: Permeability calibration chart issued by New England Research.

3.4 High Resolution Photography

High resolution photographs were taken of the study area using a Nikon D70-S digital SLR camera. There were several lenses used to collect images such as an 18-70 mm lens that was used to capture images in great detail while a 70-200 mm lens was used to capture images from a distance. Three hundred still images of sedimentary structures, faults, bar forms, and the cliff face were compiled into an image library. Images of the cliff face were chosen to be merged together using software to create a high resolution panorama of the 400 m long cliff face.

3.5 LiDAR

In this study, an Optech ILRIS-3D intelligent laser imaging system was used to acquire an ultra-high-resolution 3D point data set of the outcrop at Cambridge Cove. The 3D data set, commonly known as a point cloud, is generated from millions of points that have been recorded by the scanner in a XYZ format. The scanner is linked wirelessly to a portable computer which allows the operator to communicate with the scanner and input the predetermined parameters for each scan. The ILRIS scanner starts each scan by producing a grid over the predetermined scan area based on the resolution input by the user. The scans at Cambridge Cove were obtained using a grid spacing of 5 mm, with a point recorded every 5 mm in the X and Y direction. The distance of each point, the Z coordinate, was calculated via two-way travel time of a laser pulse from the scanner to the outcrop and back to the scanner. It is important to note that the scanner records the intensity value of the returning laser reflection and assigning each point a value on a black and white scale. This reflected intensity value could be associated with lithology (Fraser, 2010), however this will not be discussed further in this thesis.

A total of two overlapping scans were collected at Cambridge Cove. Each scan contains several sub-scans, which were digitally stitched together to form one large-scale 3D representation of the outcrop at Cambridge Cove.

3.6 Polyworks

Processing of the 3D LiDAR data was performed using Innovmetric's 3D modeling software, PolyWorks version 11. PolyWorks is designed to align, edit, and view 3D data using three of its sub modules:IMalign, IMedit, and IMSurvey, respectively.

LiDAR data were uploaded into IMalign and was translated into a coarse 3D point cloud, representative of the outcrop. IMalign then analyzed each scan and identified the orientation in which the scan was conducted in relation to the other uploaded scans. When this process was completed for every scan at Cambridge Cove, IMalign then merged the scans together to form a complete 3D image of the study area. IMalign then searched for redundant data points due to overlap, and deleted them to reduce sources of error within the other modules of Polyworks.

Once the 3D image of the outcrop was rendered, it was then imported and edited using PolyWork's IMedit module to delete outlying points and vegetation. Due to limitations within the scanner control program, LiDAR often collects data that is not within the study area (Fig. 3.3) and needs to be removed to simplify interpretation and decrease file size. Due to the nature of the study area, vast amounts of data were collected due to over shooting the sides of the cliff sections. Two hundred metres of outlying LiDAR data was collected on either side of the study area and was deleted within the IMedit module. Trees, boulders, and small shrubs include other data that were deleted. The resulting image was more clear, which helped produce an accurate interpretation (Fig. 3.4).

Post processing analysis of the LiDAR data was performed using the IMSurvey module which allowed the 3D image to be viewed at maximum resolution by directing more computer power to render a smooth and crisp 3D image.

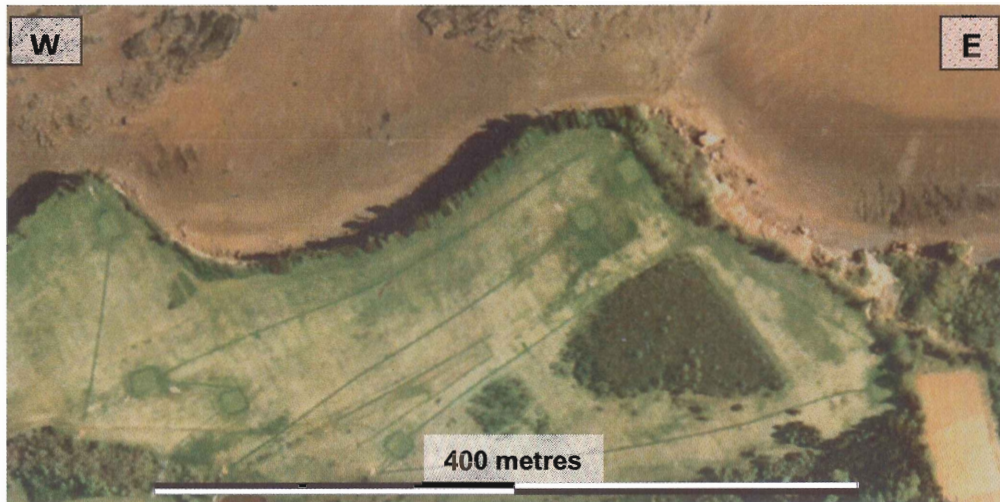


Figure 3.2: Aerial photograph of study area (Monette, unpublished).

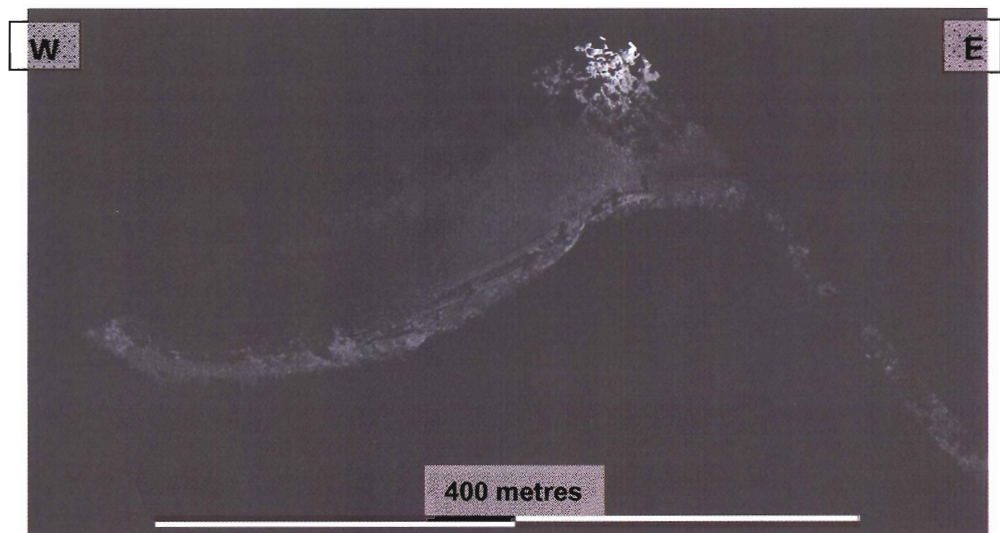


Figure 3.3: Pre-edited aerial LiDAR image of study area. (same orientation as Fig. 3.2)

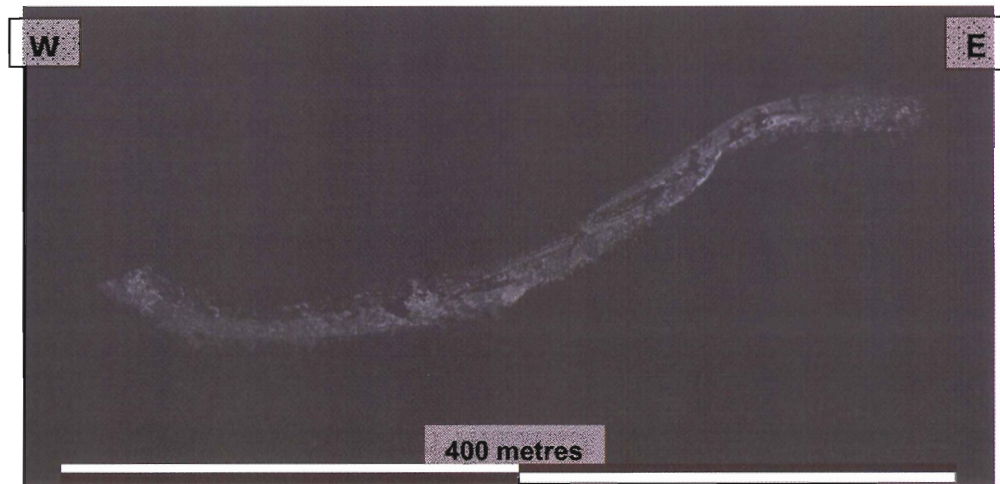


Figure 3.4: Post-edited aerial LiDAR image of study area. (same orientation as Fig. 3.2)

4.0 Results

This chapter will present the results of measured sections, gamma scintillometer readings, high resolution photography, and post-processed 3D LiDAR images. Data allowed the interpretation of: 1) the nature of deposition of the Wolfville Formation, and 2) the information to define the geometry of the bedforms and architectural elements, for input into the geological model for reservoir characterization.

4.1 Outcrop and Measured Section Descriptions

The study area at Cambridge Cove is 400 metres long and it was decided to measure five sections across the outcrop for photopan and LiDAR scan calibration, and to capture the changes in bedform architecture and geometry. This section will describe each measured section including physical sedimentary structures, grain size, lithology, as well as bed and bedset thicknesses. Measured sections are numbered 1 through 5, from west to east (Fig. 4.1).

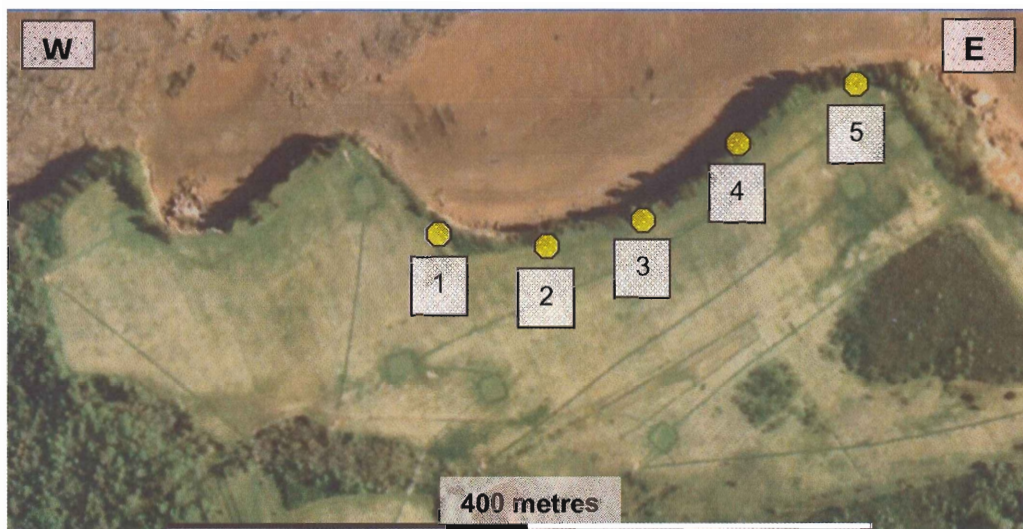


Figure 4.1: Aerial view of the Cambridge Cove study area showing measured section locations (modified from Monette, unpublished).

4.1.1 Lithofacies Descriptions

Four lithofacies were identified in the lower 20m section of the Wolfville Formation and a description of each lithofacies will be cross-referenced with Miall's (1978) facies classification (Table, 2.2).

Lithofacies 1: Clast-supported conglomerate

The clast-supported conglomerates are comprised of poorly sorted, well rounded to sub angular clasts (45-90%), ranging in size from 1cm up to 20 cm. Miall's facies classification of this lithofacies include Gm, Gt, and Gp. Barforms (Fig. 4.3) demonstrates the sedimentary structures associated with these facies codes such as horizontal bedding and imbrication (Gm), trough cross beds (Gt), and planar cross beds (Gp). Clasts included a variety of lithologies including slate, quartzite, and granite (Fig. 4.2). The matrix of this conglomerate was determined to be coarse-grained sandstone and is highly cemented with calcite. The clast-supported conglomerates found at Cambridge Cove were deposited as bar forms ranging in size from 0.5 to 2 metres thick and up to 40 metres in length. These sedimentary structures were identified as fluvial barforms. Figure 4.3 illustrates a barform with a characteristic long oval shape. Large clasts tend to be deposited on the stoss side and the smaller clasts to be deposited on the lee side of the barform. Other deposits of the clast-supported conglomerate found in the cliff sections were interpreted as deposits of channel fill, sometimes up to 3m thick. The sediments in these channel fill deposits were found to fine upwards.



Figure 4.2: Lithofacies 1- Clast-supported conglomerate at Cambridge Cove (Lens cap is 5cm diameter).

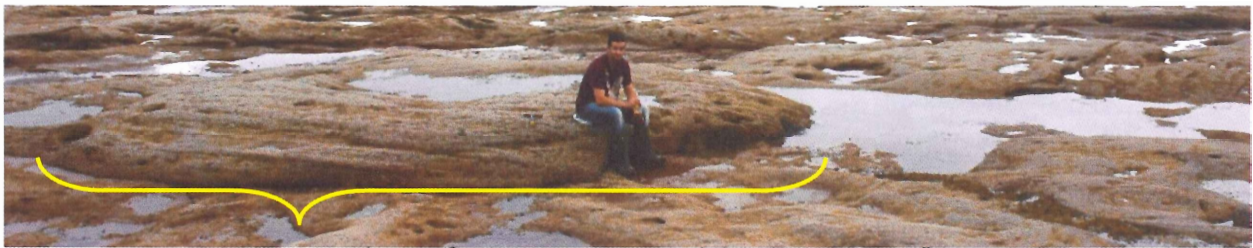


Figure 4.3: 10m barform comprising clast-supported conglomerate, lithofacies 1.

Lithofacies 2: Matrix-supported Conglomerate

The matrix-supported conglomerate is comprised of 25-45% poorly sorted, well rounded to subangular clasts, ranging in size from 1 - 20 cm (Fig 4.4). Miall's facies classification of this lithofacies include Gm, Gt, Gp, and St, are found within the matrix-supported conglomerate facies at Cambridge Cove.. Figure 4.4 and 4.5 demonstrate the sedimentary structures associated with these facies codes, including horizontal bedding and imbrication (Gm), trough cross beds (Gt), and planar cross beds (Gp). These clasts include a variety of lithologies, including slates, quartzite, and granite. The matrix of this conglomerate is composed of calcite cemented coarse-grained sandstone.. The matrix-supported conglomerate at Cambridge Cove was deposited in a barform architecture. The barforms dimensions range from 0.5 – 3.0 m thicknesses

and are as long as 20 m.. This lithofacies contains structural features such as trough cross-bedding and low-angle (10°) cross-bedding (Fig. 4.5).



Figure 4.4: Matrix-supported Conglomerate lithofacies-2 at Cambridge Cove (lens cap is 5cm).

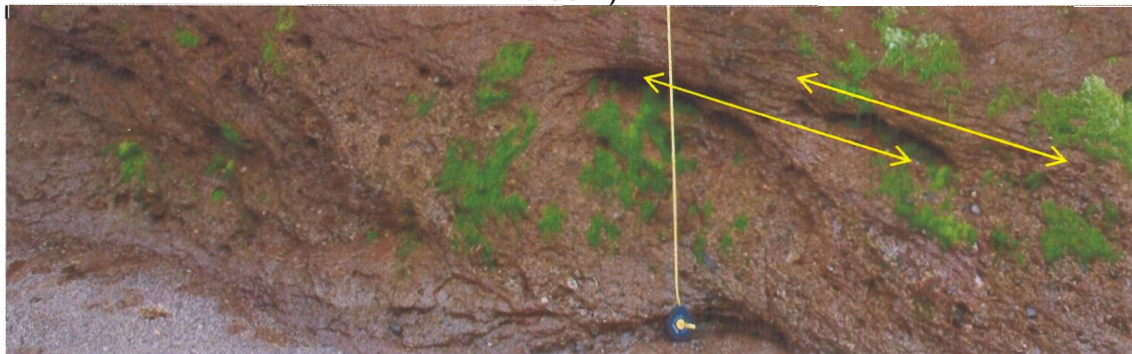


Figure 4.5: Low angle (10°) cross-bedding in matrix-supported conglomerate, lithofacies2 **Lithofacies 3: Sandstone**

Red sandstone layers found at Cambridge Cove form laterally continuous beds, 30-70 cm thick (Fig. 4.6). Miall's facies classification of this lithofacies includes St, Sp, Sh, and Sl. Figure 4.4 and 4.5 demonstrate the sedimentary structures associated with these facies codes, including solitary or grouped trough cross beds (St), solitary or grouped planar cross beds (Sp), horizontal lamination (Sh), and low angle cross beds (Sl). Lithology of this sandstone is dominantly quartz with some feldspar and occasional

metasediment grains. Textures range from fine-to coarse-grained, rounded to sub angular, and very well sorted. Large pebble- to -cobble sized clasts were found within the sandstone, 5 to 20cm in size, and mainly metasediment and granite. Physical sedimentary structures within the sandstone beds includes subhorizontal to low-angle planar cross-strata. There are occasional beds of trough cross-bedding.

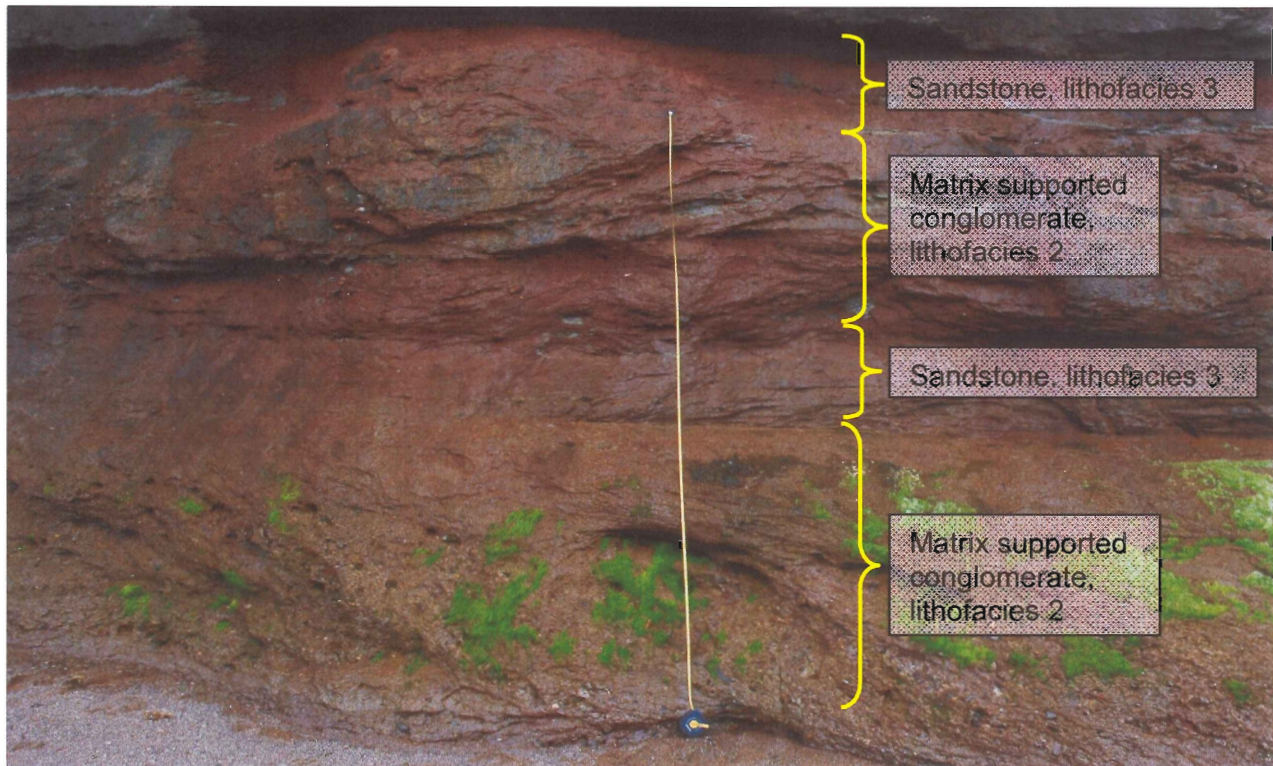


Figure 4.6: Sandstone lithofacies 3 and matrix supported conglomerate lithofacies 2, at Cambridge Cove. Scale is 2.5 metres (note tape measure).

Lithofacies 4: Paleosols

Paleosols at Cambridge Cove consist of thin horizons of carbonate-bearing sediment at the top of laterally extensive sandstone beds. These form isolated carbonate nodules within fine-grained sand and silt horizons, which indicates paleosol development (Leleu et al., 2009). Vertical and horizontal mottling, which are dominantly dark gray color, is attributed to traces of rooting of ancient plants (Klappa, 1980). The

upper contact of the paleosol horizon is erosional, which is now underlies the clast-supported (lithofacies 1), and matrix-supported conglomerate (lithofacies 2).

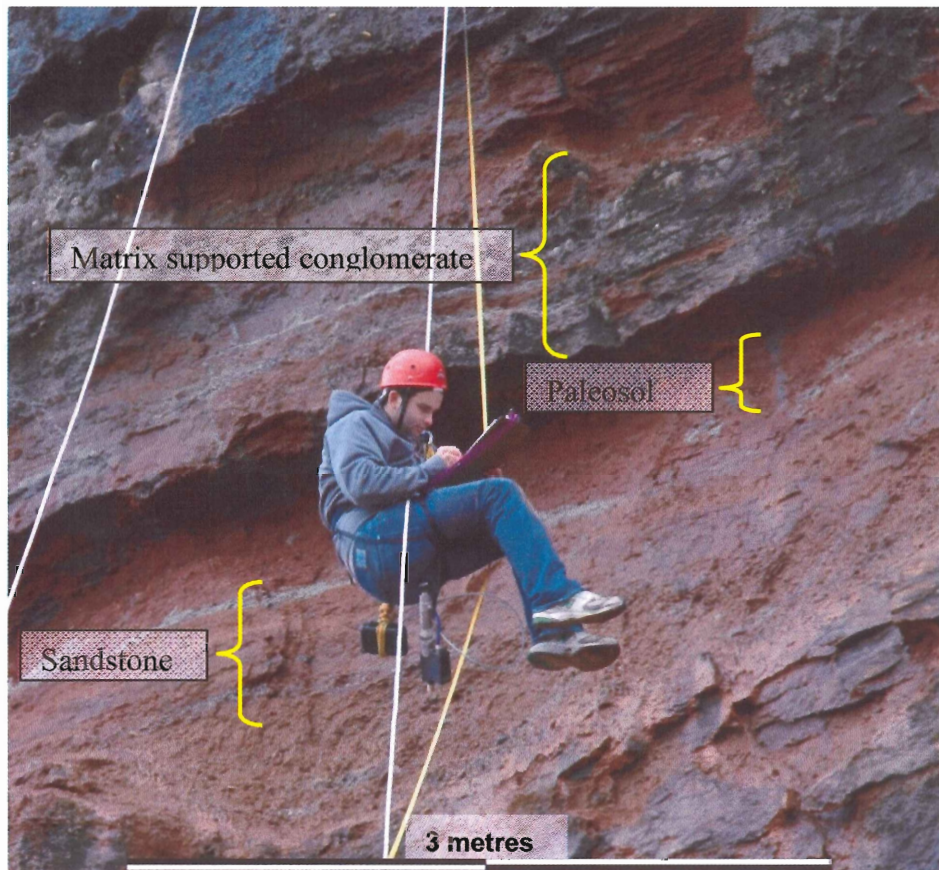


Figure 4.7: Paleosol (lithofacies 4) horizon displaying vertical and horizontal traces attributed to rooting, terminated by erosional surface and matrix-supported conglomerate.

4.1.2 Depositional Cycles

The depositional cycles at Cambridge Cove commence with a sharp erosional surface in which clast-supported and matrix-supported conglomerates were deposited. Each cycle fines to a thick layer (~1metre) of medium-coarse grained sandstone and is capped by a thin paleosol horizon. Cycles within this depositional environment were possibly driven by mechanisms including tectonic activity, climate change, and seasonal effects, coupled to accommodation space (Gibling, 2006). As described by Hubert and

Forlenza (1988), their facies correspond to facies Gm and Sh of Miall (1978), and are found to dominate the cycles. The facies is capped by planar bedded sandstones, commonly composed of carbonaceous material with root casts. These cycles are a defining feature of braid channel deposits and are formed as the river channels migrate laterally, resulting in the deposition of vertical and horizontal stacked bar deposits and bedload sheets (Gibling, 2006).

4.1.3 Section 1

Measured section 1 is located on the extreme west end of the outcrop and has a total measured thickness of 21 m. The measured section was broken down into three depositional cycles, which are marked by a major erosional surface at the base and a medium-to coarse-grained sandstone layer, including paleosol, at the top of each cycle (Fig. 4.8). Each cycle was investigated, It was observed that each cycle contained four main lithofacies; clast-supported conglomerates, matrix-supported conglomerates, medium-coarse grained sandstones and paleosols.

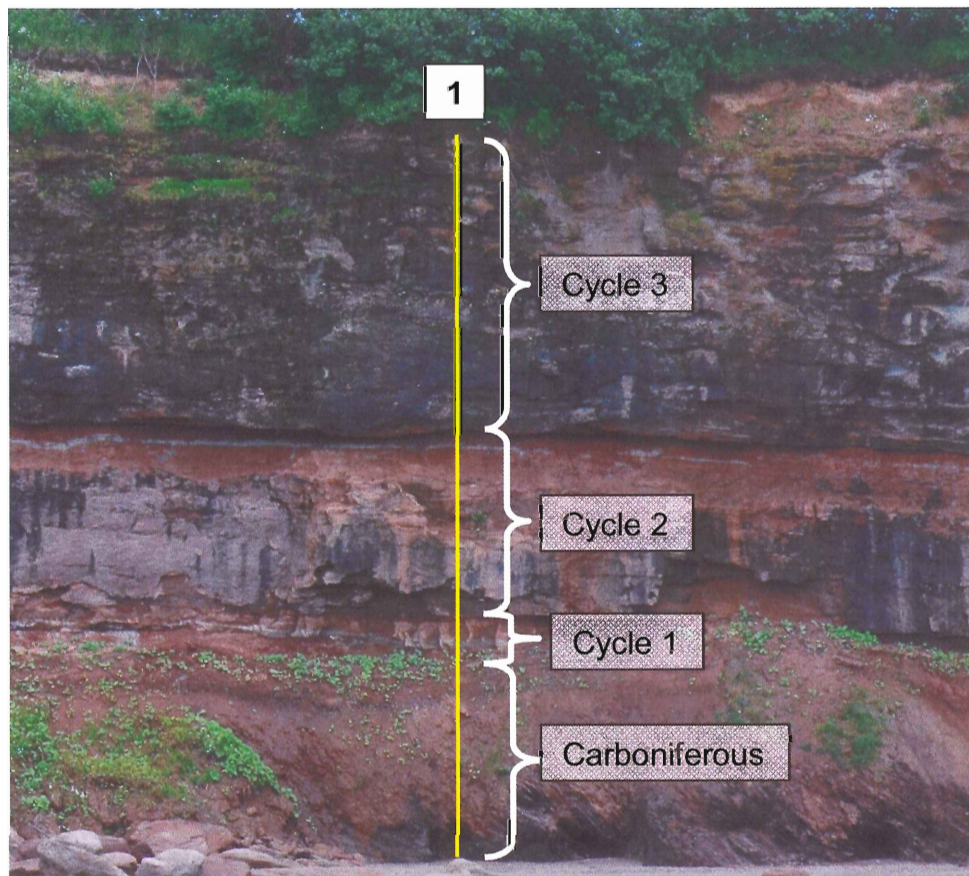


Figure 4.8: Measured section #1 divided into three depositional cycles.

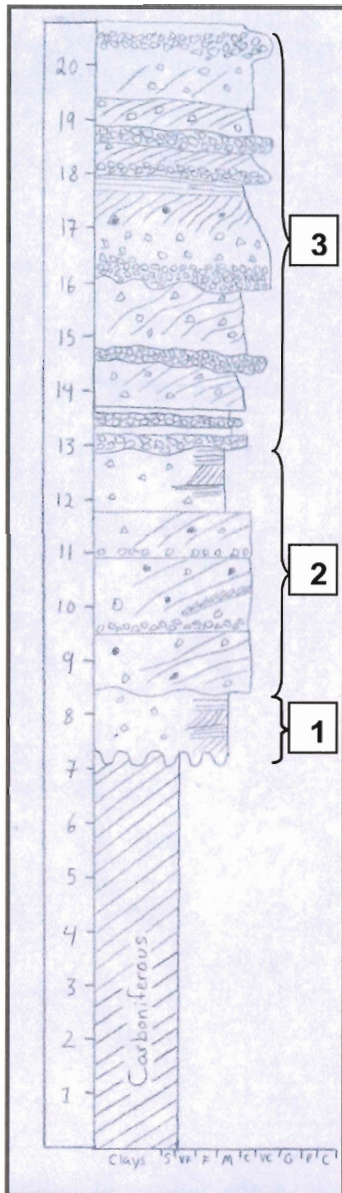


Figure 4.9: Measured section #1.

Figure 4.9 is a stratigraphic log of section 1 and displays the stratigraphic complexity found within the measured section. Described from the bottom of the section to the top, we can see that the basal strata is 7 ms of Carboniferous Horton Bluff Formation shales. Directly above the Carboniferous material we encounter the oldest Triassic depositional cycle with a measured thickness of 1.5 m. This section only contains a sandstone layer. Cycle 2 was deposited directly above cycle 1 on an erosional surface. The bottom 3.5 metres of this cycle comprises matrix-supported conglomerate deposited as sheet-like beds that range in thickness from 0.5 to 1 m. Each bed is separated by erosional surfaces. The three beds found in cycle 2 contain well rounded clasts that range in size from 1-10 cm and imbrications features are noted. Each bed tends to fine upwards from 20% to 30% clasts at the base, to 5% to 10% clasts at the top. The matrix consists of coarse- to very coarse-grained sandstone. The top of cycle 2 ends with 1 m of coarse-grained sandstone with some signs of early paleosol formation

which include some carbonaceous sediment and probable root mottling. Cycle 3 contains several beds of matrix dominant conglomerate and clast dominant conglomerate. Like cycle 2, the matrix dominant conglomerate beds were deposited in sheet-like beds that range in thickness from 0.5 to 1 metres, show signs of imbrication,

and fine upward. Cycle 3 contains 7 thin beds of clast dominant conglomerate that consist almost entirely of well rounded clasts (80% to 95% clasts).

4.1.4 Section 2

Measured section 2 is similar to section 1 as it contains three depositional cycles (Fig. 4.10); however, the stacking patterns within each cycle have changed. This could be due to localized channel abandonment during deposition. There is a total measured thickness of 20 m. The upper 14 m is the Wolfville Formation.

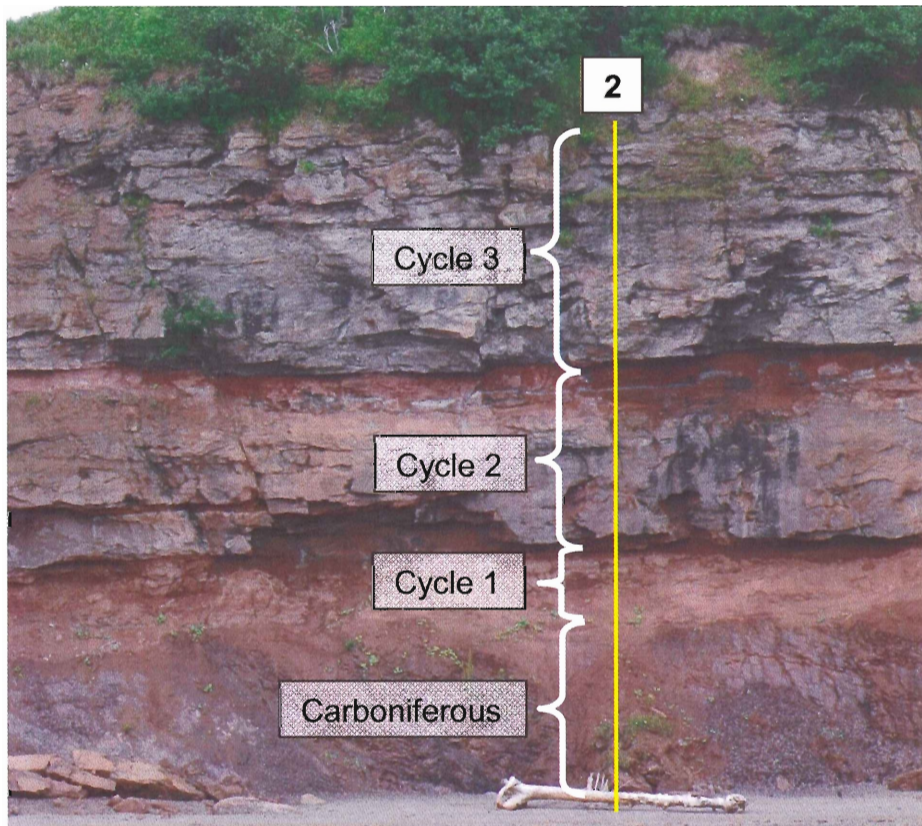


Figure 4.10: Measured section #2 divided into three depositional cycles with the basal Carboniferous Horton Group and the overlying Wolfville Formation.

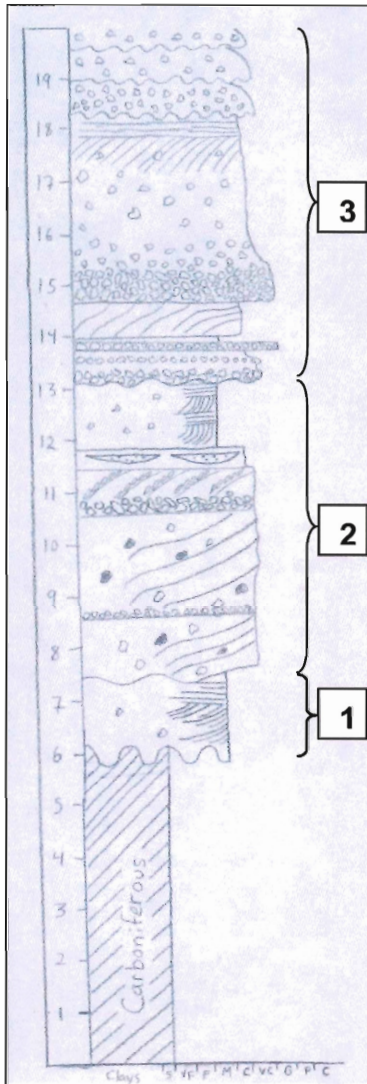


Figure 4.11: Measured section #2.

The second stratigraphic section, Figure 4.11, contains three main depositional cycles that lie uncomfortably above 6 m of Carboniferous shale and mudstone. Cycle 1 is incomplete and only and contains 1 metre of well sorted coarse-grained sandstone. Cycle 2 was deposited on a slight erosional surface, and contains four sheet-like beds of matrix dominant conglomerate. Each sheet of conglomerate was deposited on a slight erosional surface, and fines upwards from 20% to 30% clast to 5% to 10% clast. The last sheet of conglomerate in this cycle is clast rich (40%) and fines up over a short distance to a coarse/pebbly sandstone. The clasts at the base of this bed were found to be highly imbricated. This cycle ends with the deposition of 1.3 m of coarse-grained sandstone, which is an indication of a early stage paleosol at the top. Sedimentary structures within the sandstone contained low angle planar cross-strata. The third cycle found in this section is comprised of matrix and clast supported conglomerate beds. The first two

beds were found to be clast-supported conglomerate, which are separated by a thin layer of coarse-grained sandstone. Clasts were 2-15 cm in size, well rounded, and were very well sorted. The clast-supported conglomerate sheet-like bed fines into a matrix-supported conglomerate and finally a coarse-grained sandstone with sporadic clasts and low angle cross-bedding capped by parallel bedding. The three final beds

recorded within this section are clast supported conglomerate that are separated by sharp erosional surfaces.

4.1.5 Section 3

Section 3 is comprised of 4 cycles and has a total measured thickness of 18 m. This measured section was much shorter due to the amount of glacial till that was located at the top and was not included in the measured section. Each cycle was investigated and it was observed that each cycle contains the four main lithofacies; clast- supported conglomerates, matrix-supported conglomerates, medium-coarse grained sandstones and paleosols. This section was different than the previous two sections as it contained a much more variable stacking pattern.

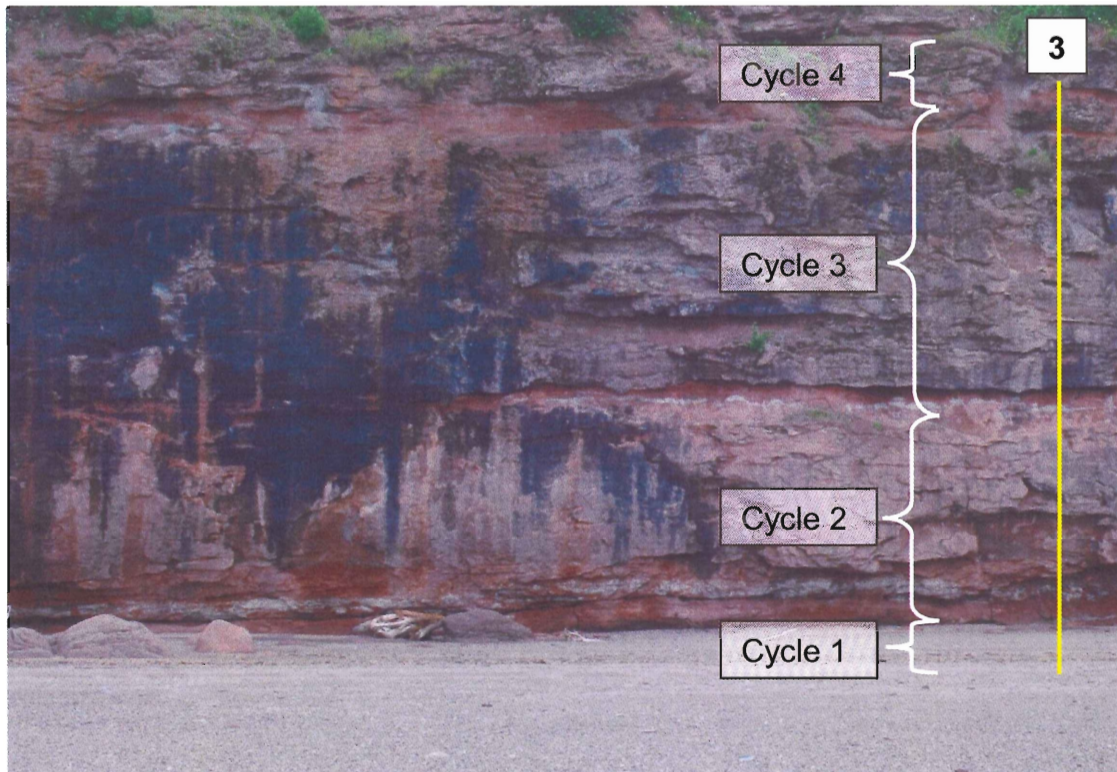


Figure 4.12: Measured section #3 divided into four depositional cycles.

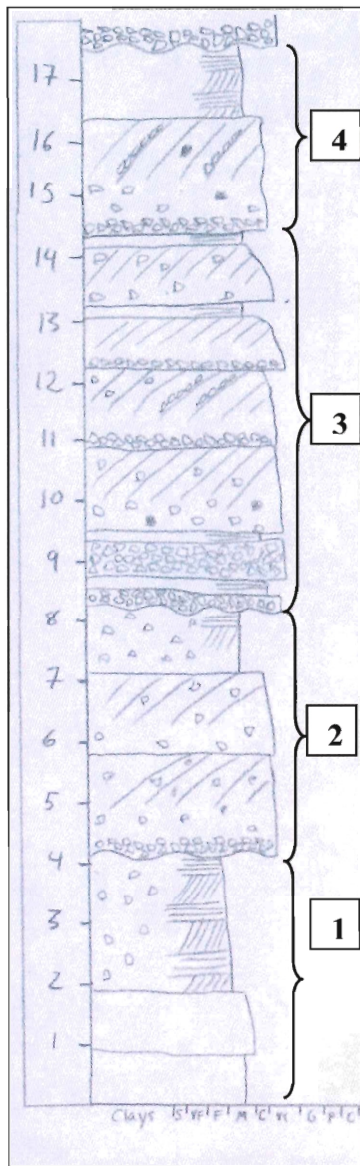


Figure 4.13: Measured section #3.

The stratigraphic section (Fig. 4.13) for the third measured section has been broken up into four depositional cycles. The first cycle contains two beds of matrix supported conglomerate with low angle planar cross-stratification. Most oclasts that are found within these beds are imbricate within the base of these low-angle sedimentary structures. This cycle is capped off with 2 m of coarse-grained sandstone that contains subtle signs of trough cross-stratification. Cycle 2 is comprised of two large beds of matrix-supported conglomerate with well sorted clasts and low angle cross-stratification. This cycle terminates with 1.2 m of coarse grained sandstone that contains a sporadic distribution of clasts (5%), and sub horizontal planar bedding. Cycle 3 contains several beds and one defined channel body. The base of this cycle begins with a sharp erosional surface and is filled with clast supported conglomerate (85-90% clasts).

This conglomerate bed is a 1 m thick channel fill deposit that contains thin inter-bedded sand drapes. The cycle ends with a very thick bed of matrix-supported conglomerate that fines into a coarse-grained sandstone with sporadic clasts. The sandstone body that marks the end of Cycle 3 is not very thick due to an erosional surface that cuts into the sandstone bed. This erosional feature marks the beginning of cycle 4. Cycle 4 is thin with clast supported conglomerate at the base and fines up into matrix-supported conglomerate. The clasts

found at the top of this bed are observed to be imbricated along low angle planar cross-stratification. The top of this cycle contains 1 m of very clean, well rounded, cross-stratified sandstone. There are some signs of paleosol formation from the observation of carbonaceous sediment at the top of the sandstone bed; however, most has been eroded away from the subsequent deposition of another cycle.

4.1.6 Section 4

Section 4 is the thickest stratigraphic section within the study area, containing 21 m of the Wolfville Formation. The section is split into 5 depositional cycles, two of which are partial cycles. This section was partially covered by iron staining (Fig. 4.14) due to the seeping of ground water out of the cliff face onto the study area. The iron staining did not affect the collection of data from the cliff face.

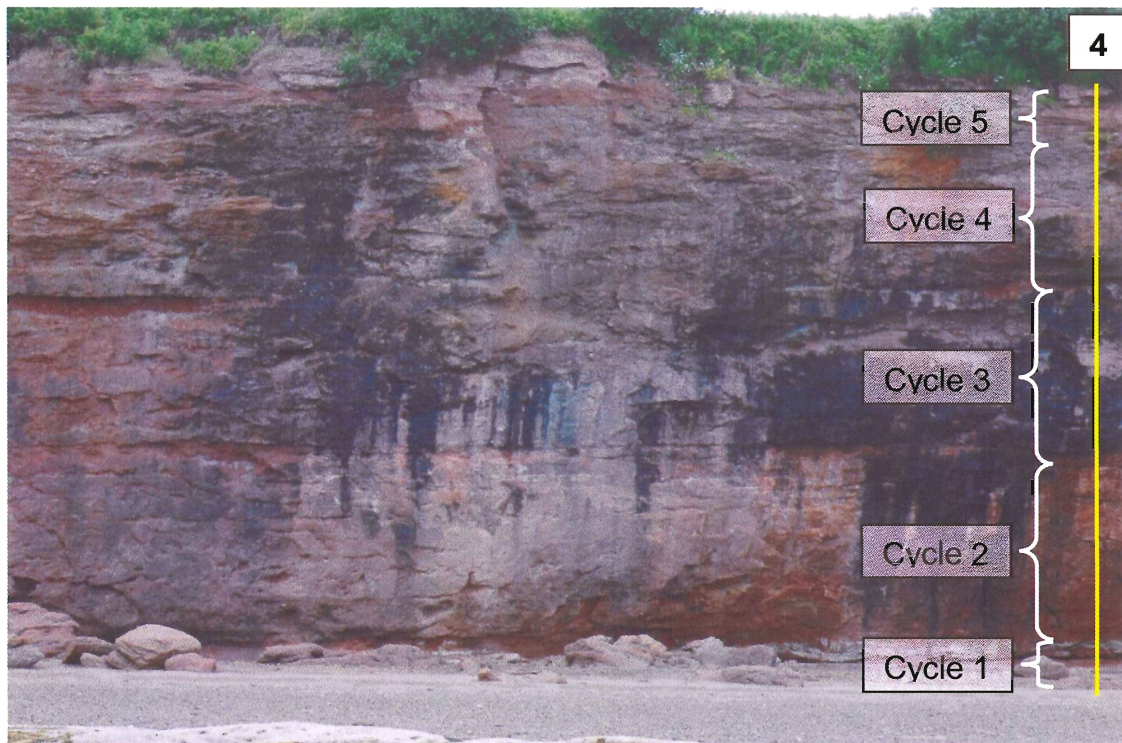


Figure 4.14: Measured section #4 divided into 5 depositional cycles. Note the black iron staining that is present across the outcrop.

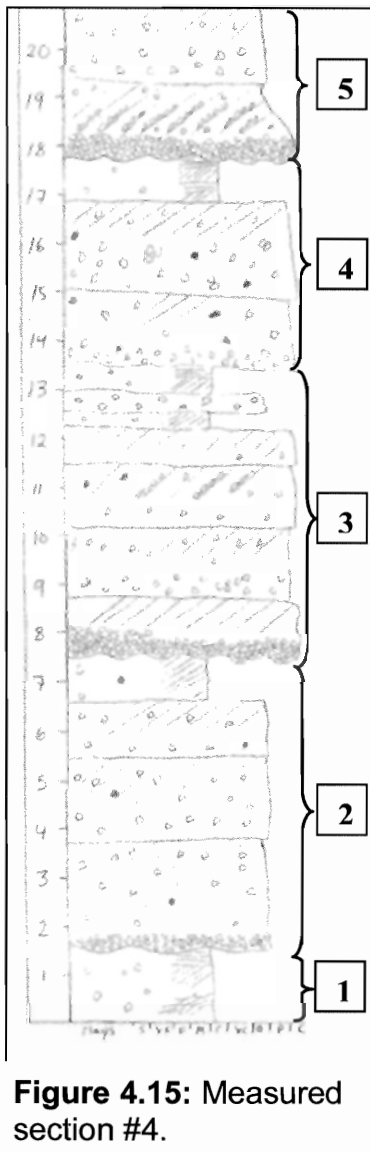


Figure 4.15: Measured section #4.

Figure 4.15 depicts the stratigraphic framework found in the fourth section, and has been divided into 5 depositional cycles. Cycle 1, an incomplete cycle, contains 1.5 m of coarse grained sandstone. This sandstone bed contains a few clasts found sporadically within the bed. This sandstone contains trough cross-bedding at the base which is truncated by a reactivation surface with low angle planar cross-bedding above. Cycle 2 starts with the deposition of clast-supported conglomerate (60-80% clasts) within an erosional scour that cuts into cycle 1. This quickly grades into a matrix-supported conglomerate with fewer clasts (20-30%). Two more beds of matrix-supported conglomerate are found in this cycle, each contain low angle planar cross-bedding. Cycle 2 ends with 0.8 m of clean medium- to coarse- grained sandstone with occasional clasts and subhorizontal parallel bedding. Cycle

3 is similar to cycle 2 as it starts with a deep erosional scour and is filled in with clast-supported conglomerate. Above this bed there is 3.5 m of matrix-supported conglomerate, separated into three beds, which are defined by erosional surfaces. There are cases of well-defined clast imbrication found within these beds. Cycle 3 is terminated by 1.5 m of coarse-grained sandstone with a thin lens of matrix-supported conglomerate. Cycle 4 is thin with 3 metres of matrix-supported conglomerate separated into two beds. Low angle planar cross-bedding was observed within these

beds. Cycle 4 ends with 0.7 m of clean, well-sorted, coarse-grained sandstone with subhorizontal planar bedding grading into parallel bedding. The 5th and final cycle is an incomplete cycle. This cycle starts out with 0.5 m of clast-supported conglomerate (80-90% clasts) that fills in a deep erosional scour. This bed fines upward into a matrix-supported conglomerate that contains imbricated clasts that lie along the planar cross trough bedding planes. The final bed of the cycle is a matrix supported conglomerate and contains some signs of cross trough planar bedding.

4.1.7 Section 5

Section 5 is the final section within the study area and is located on the far east of the cliff section. Figure 4.15 illustrates this 18 m thick section, and the four depositional cycles observed in the bedding..

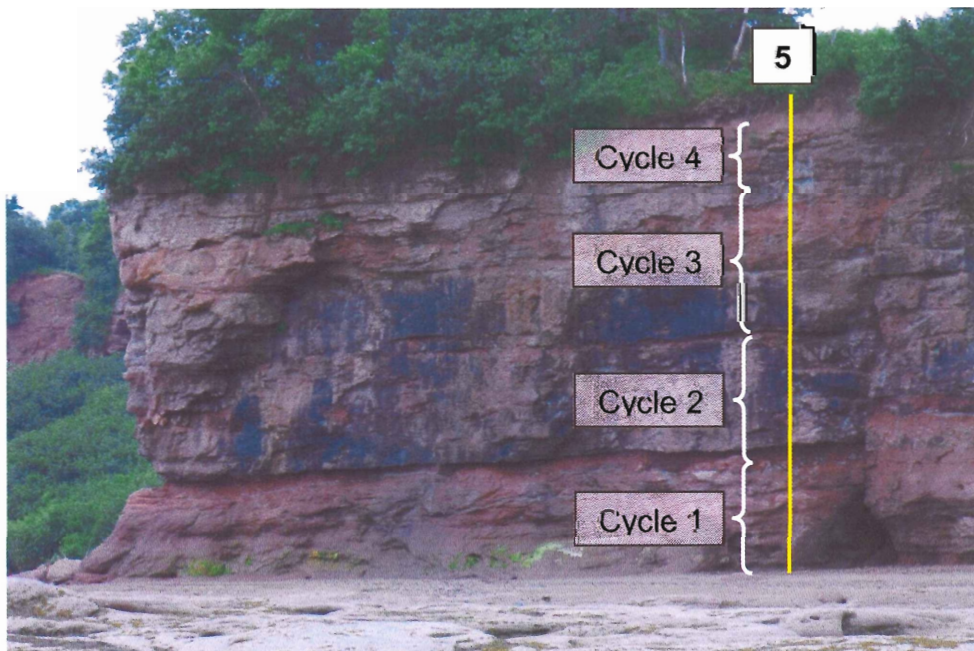


Figure 4.16: Measured section #5, divided into 4 depositional cycles.

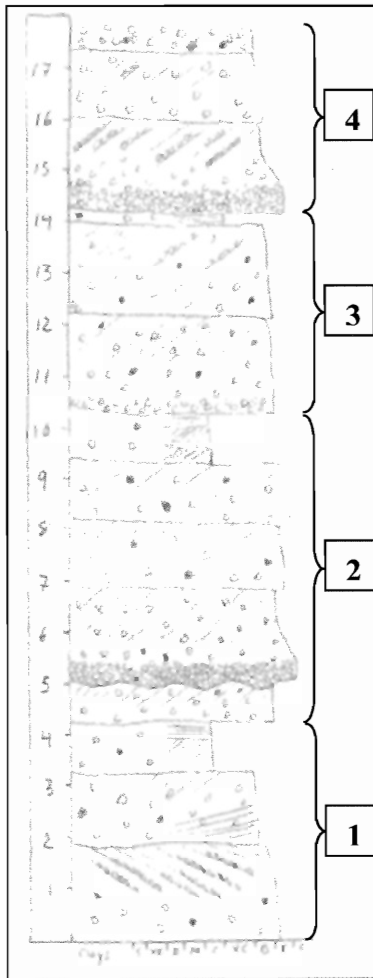


Figure 4.17: Measured section #5.

Figure 4.17 illustrates the 5th stratigraphic section which contains 18 m of Wolfville Formation. This section is broken into four depositional cycles, two of which are incomplete. Cycle 1 begins with 3 m of matrix-supported conglomerate, which are separated into 2 different beds by an erosional contact. The first bed of conglomerate features low angle cross-stratified planar beds with imbricate clasts. The clasts in this bed dip in a different direction than the beds above, possibly due to a shift in depositional direction within the channel body. The second bed contains subhorizontal planar bedding that grades into higher-angle cross trough bedding. This cycle ends with 1 m of coarse-grained sandstone with subhorizontal planar bedding.

Cycle 2 begins with a small bed of matrix-supported conglomerate capped by a sharp erosional scour. This is

in-filled with a bed of clast-supported conglomerate (80-90% clasts) that fine upwards into a matrix-supported conglomerate (30-50% clasts). There are two more beds of matrix-supported conglomerate that are capped with a 1 m thick bed of clean, coarse-grained sand. This sandstone bed contains some signs of trough-cross bedding which eventually develops into subhorizontal bedding at the top. Cycle 3 is similar, containing two beds of matrix-supported conglomerate that fines into a coarse-grained sand at the top, which ends cycle 3. Cycle 4 is chaotic; it starts with the deposition of a clast-supported conglomerate within a deep erosional feature that cuts into cycle 3. This

conglomerate bed becomes less chaotic and clasts are found to be imbricated along low angle planar bedding. The final bed in cycle 4 is a matrix-supported conglomerate that contains some minor signs of low angle cross-stratified planar bedding.

4.2 Gamma readings

During analysis of the 1st stratigraphic section, a gamma scintillometer was strapped to the rock climbing gear and a gamma log was recorded. Figure 4.18 illustrates the gamma curve compared to stratigraphic section 1.

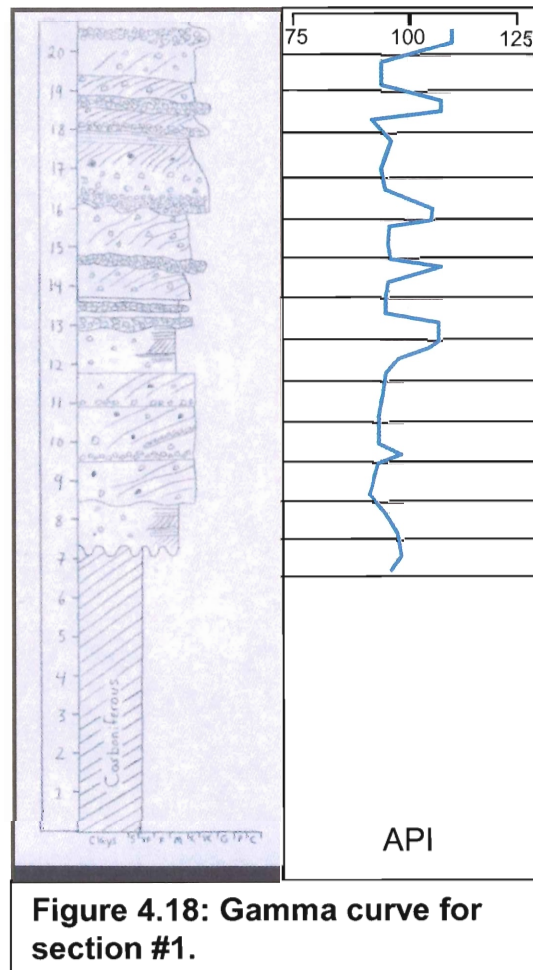


Figure 4.18: Gamma curve for section #1.

4.3 Permeability

The lithologies found within the Wolfville Formation were found to be highly cemented and it was difficult to obtain correct permeability results. Due to the nature of the conglomerates (large clast sizes), the hand held permeameter could not create an air-tight seal against the rock face, thus losing pressure and displaying incorrect results. The only lithology that displayed accurate, consistent results was the laterally extensive sandstone beds. During the collection of the 2nd stratigraphic section, samples of each sandstone layer encountered were hammered off the cliff face and were tested for permeability values. Table 4.1 displays the permeability results obtained at Cambridge Cove, and the sample locations are illustrated in Figure 4.19.

No.	Height	Permeameter value	Permeability (mD)
1	18 metres	11.32	70mD
2	12.5 metres	10.76	350mD
3	7metres	10.49	800mD

Table 4.1: Permeability values obtained from stratigraphic section 2.

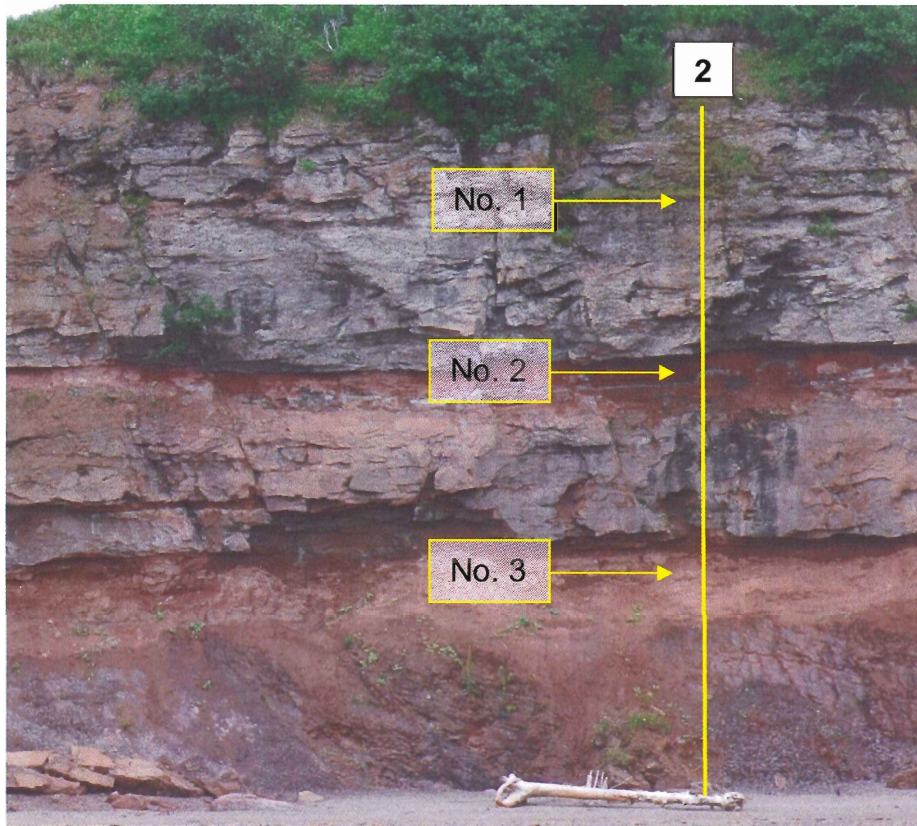


Figure 4.19: Locations of permeability tests on stratigraphic section #2.

4.4 High Resolution Photogrammetry

Using the still photos taken with the Nikon D70, a composite photopan was created of the entire cliff face which allowed for the identification and mapping of all the major channel bodies and barforms within the cliff face. Once the channels and barforms were identified and isolated within the photo pan, it was cross referenced with the LiDAR data to provide reference points for measuring the channel and barform widths and heights. Section 4.5 will demonstrate the results of the amalgamation of the high-resolution photography with the LiDAR data by providing tables with accurate measurements of channel bodies and barforms.

4.5 LiDAR

LiDAR data in conjunction with high resolution photogrammetry highlights the channel bodies and associated barforms found within the outcrop. Due to the large size of the study area, the cliff face is sectioned off into four 100m segments to display the results in higher resolution. Figure 4.20 displays how the study section has been divided. Each segment features a composite photo pan (Fig. 4.21 to 4.28) with the outlined channel bodies and associated barforms which is cross referenced with the LiDAR data to perform accurate measurement of both the width and thicknesses (W/T) of these architectural elements. A table is provided for each segment displaying the widths and thicknesses of each architectural element.

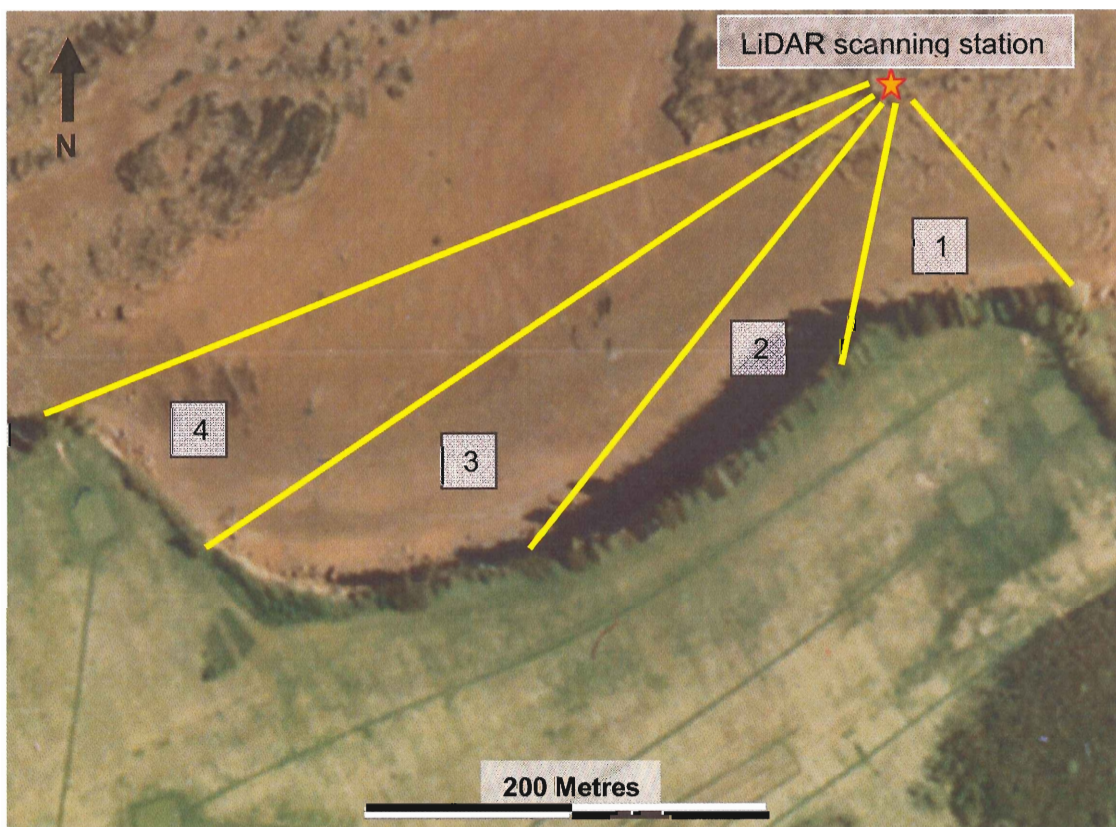


Figure 4.20: Cambridge Cove study area divided into 100 m sections for Li processing (modified from Monette, 2008).

4.5.1 Section 1

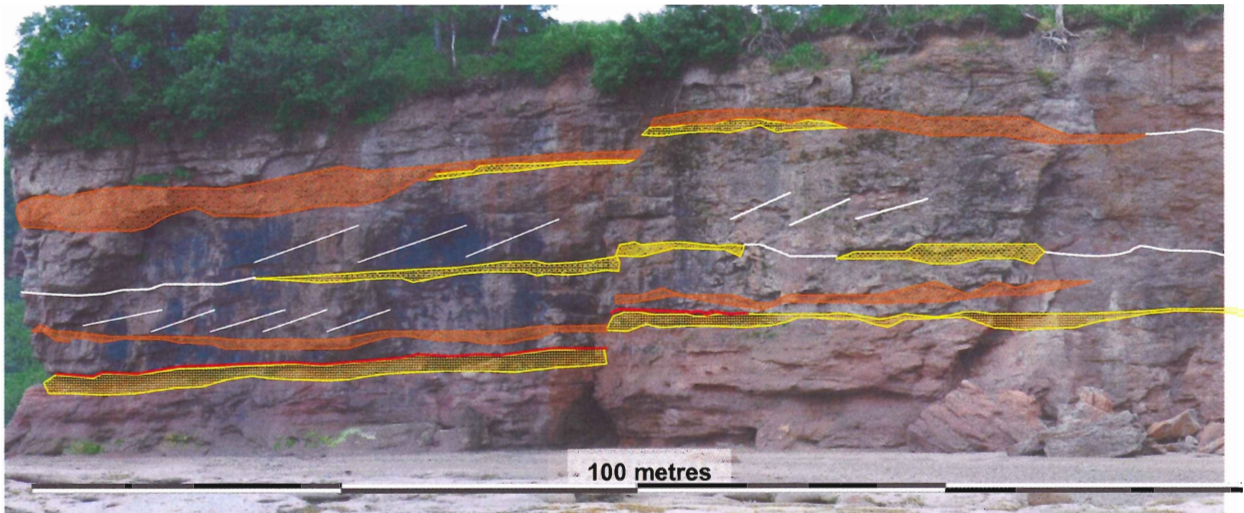


Figure 4.21: Composite photopan of section 1 displaying architectural elements.

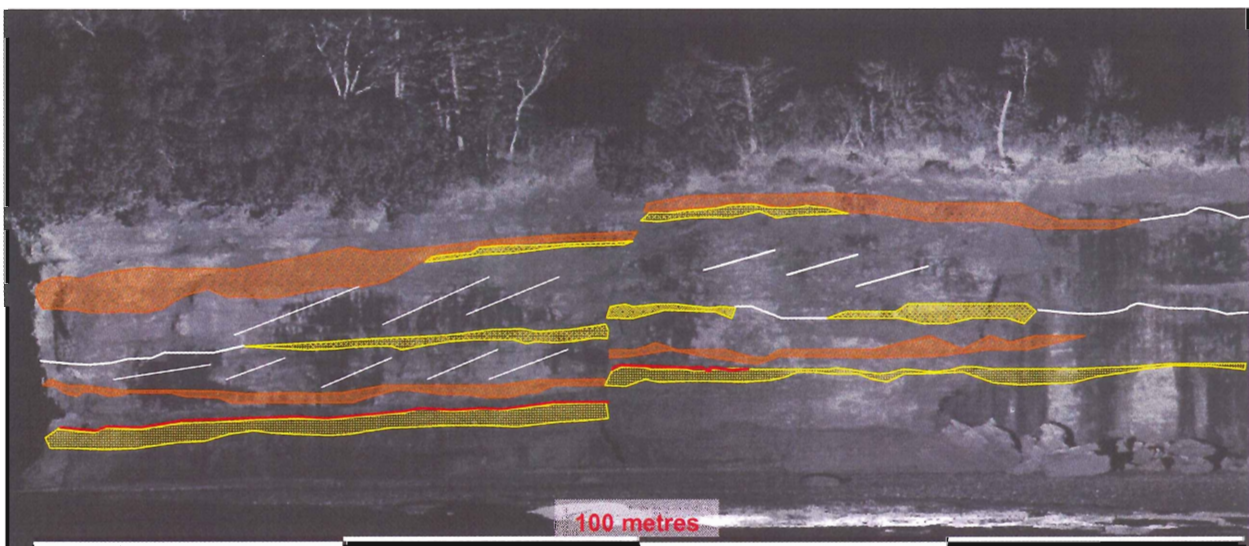


Figure 4.22: LiDAR image of section 1 used to accurately measure architectural elements.

Color	Lithofacies	Architectural elements	Width	Thickness
Orange	1	channel bodies	>50m	<1m
White outline	2	barforms	>100m	<3m
Yellow	3	medium- to coarse-grained sandstone Beds	>100m	<1m
Red	4	paleosols	>50m	<0.5m

Table 4.2: Architectural elements found in section 1.

4.5.2 Section 2

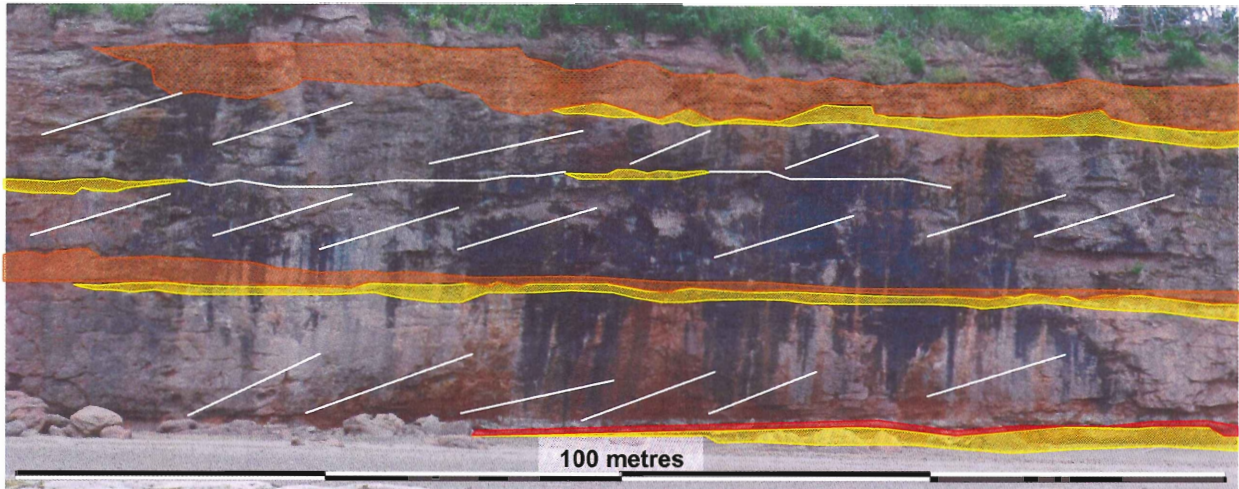


Figure 4.23: Composite photopan of section 2 displaying architectural elements.

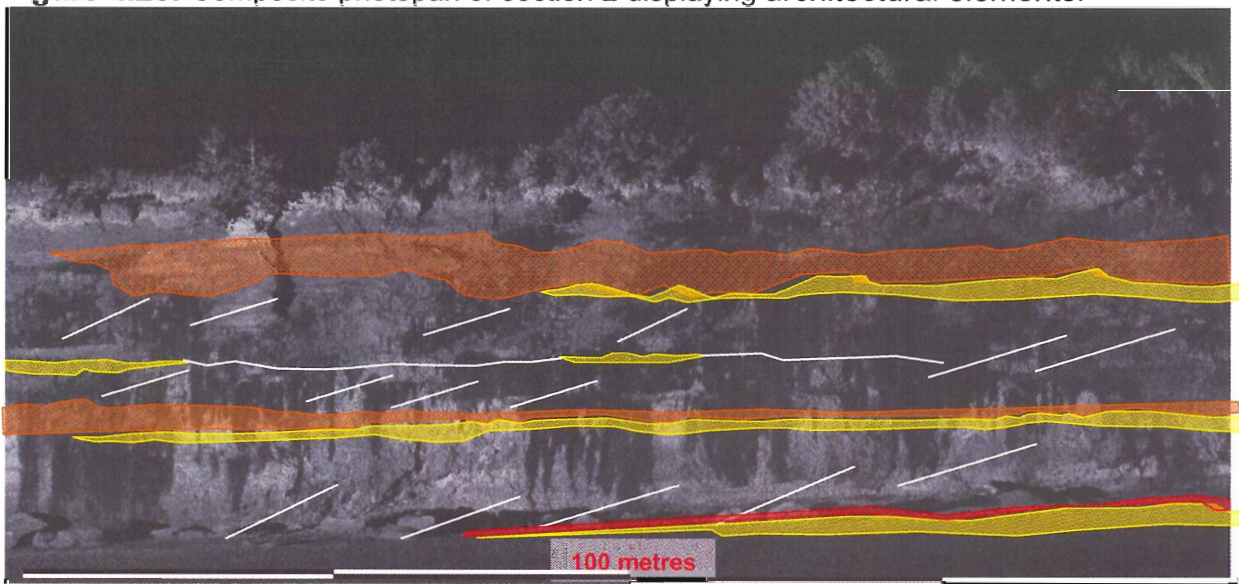


Figure 4.24: LiDAR image of section 2.

Color	Lithofacies	Architectural elements	Width	Thickness
Orange	1	channel bodies	>100m	<2m
White outline	2	barforms	>100m	<5m
Yellow	3	medium- to coarse- grained sandstone Beds	>100m	<1m
Red	4	Paleosols	>50m	<0.5m

Table 4.3: Architectural elements found in section 2.

4.5.3 Section 3

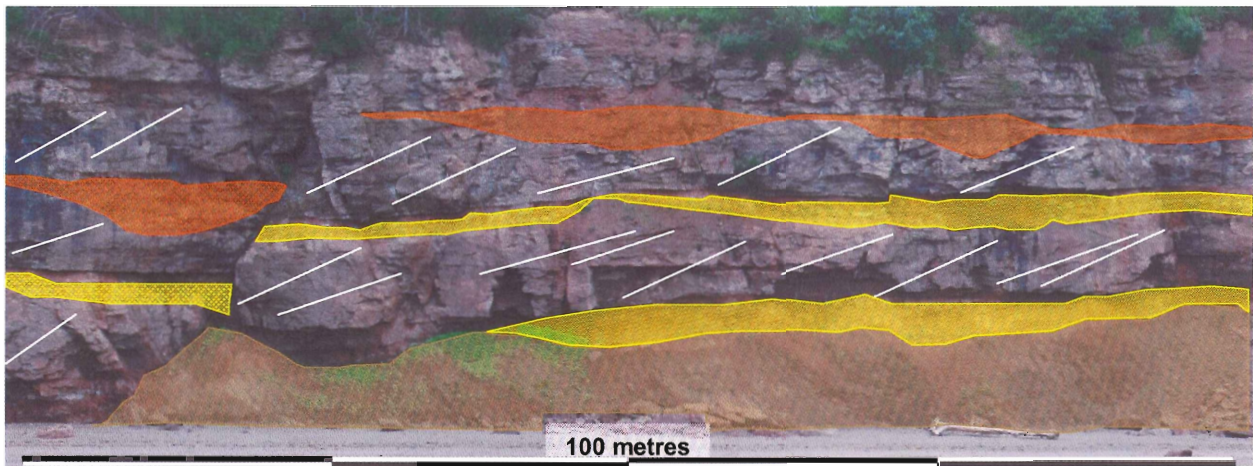


Figure 4.25: Composite photopan of section 3 displaying architectural elements.

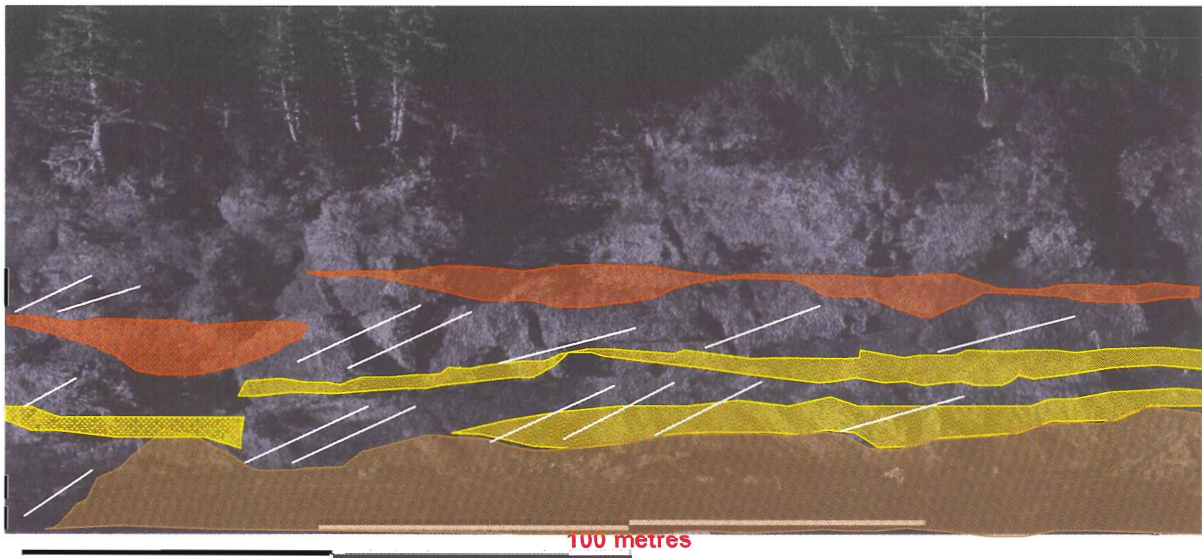


Figure 4.26: LiDAR image of section 3.

Color	Lithofacies	Architectural elements	Width	Thickness
Orange	1	channel bodies	>100m	<1.5m
White	2	barforms	>100m	<3m
Yellow	3	medium- to coarse- grained sandstone Beds	>100m	<1m
Red	4	paleosols	0	0
Brown	NA	carboniferous	NA	NA

Table 4.4: Architectural elements found in section 3.

4.5.3 Section 4

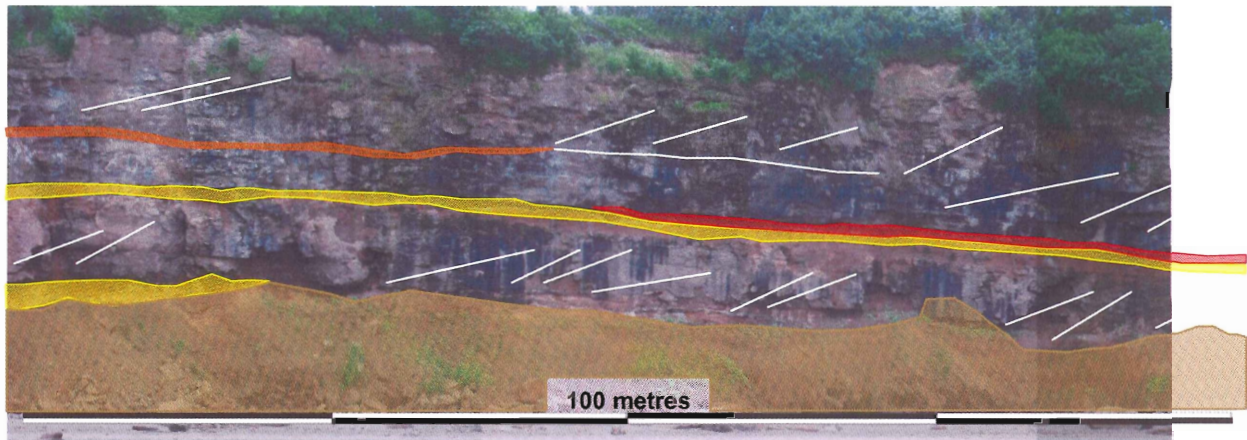


Figure 4.27: Composite photopan of section 3 displaying architectural elements.

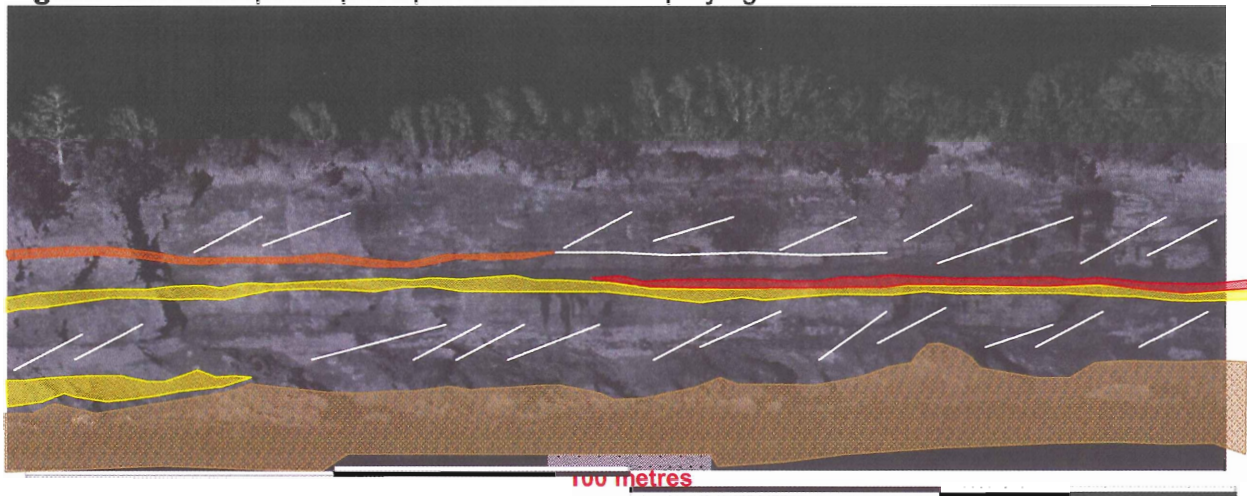


Figure 4.28: LiDAR image of section 4.


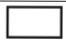



Color	Lithofacies	Architectural elements	Width	Thickness
	1	channel bodies	<40m	<0.5m
	2	barforms	>100m	<3m
	3	medium- to coarse-grained sandstone Beds	>100m	<1m
	4	paleosols	>50m	<0.5Mm
	NA	carboniferous	NA	NA

Table 4.5: Architectural elements found in section 4.

4.5.2 Faults

There were 4 major faults and 7 minor faults observed within the Cambridge Cove study area. Major faults were defined as having more than 0.5 m vertical offset, minor faults as having negligible vertical displacement. The faults at Cambridge Cove are normal faults reflecting the extensional nature of the basin. Figure 4.28 depicts the location of each major fault, and Table 4.6 describes each major fault. Figure 4.29 is a LiDAR image with all major faults (red) and the minor faults (blue) plotted as planes.

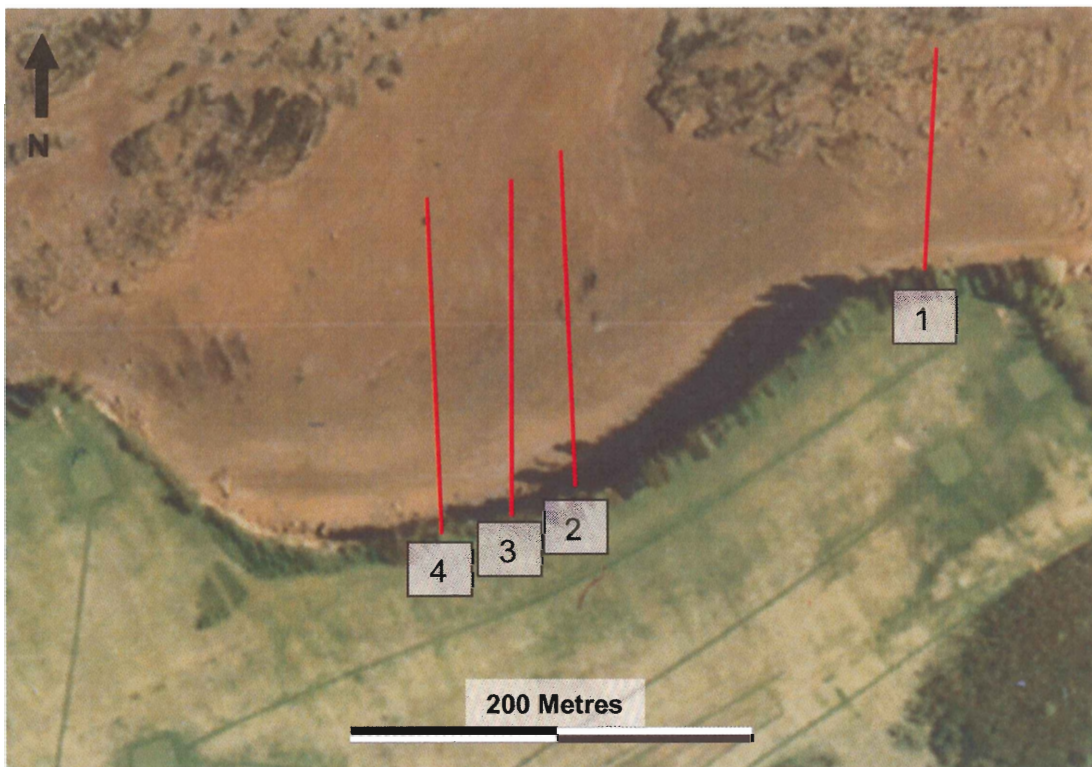


Figure 4.29: Aerial view of the Cambridge Cove study area showing the locations of the major faults (modified from Monette, 2008).

Fault	Strike	Dip
1	007°	82°
2	358°	80°
3	004°	67°
4	358°	62°

Table 4.6: Major fault description

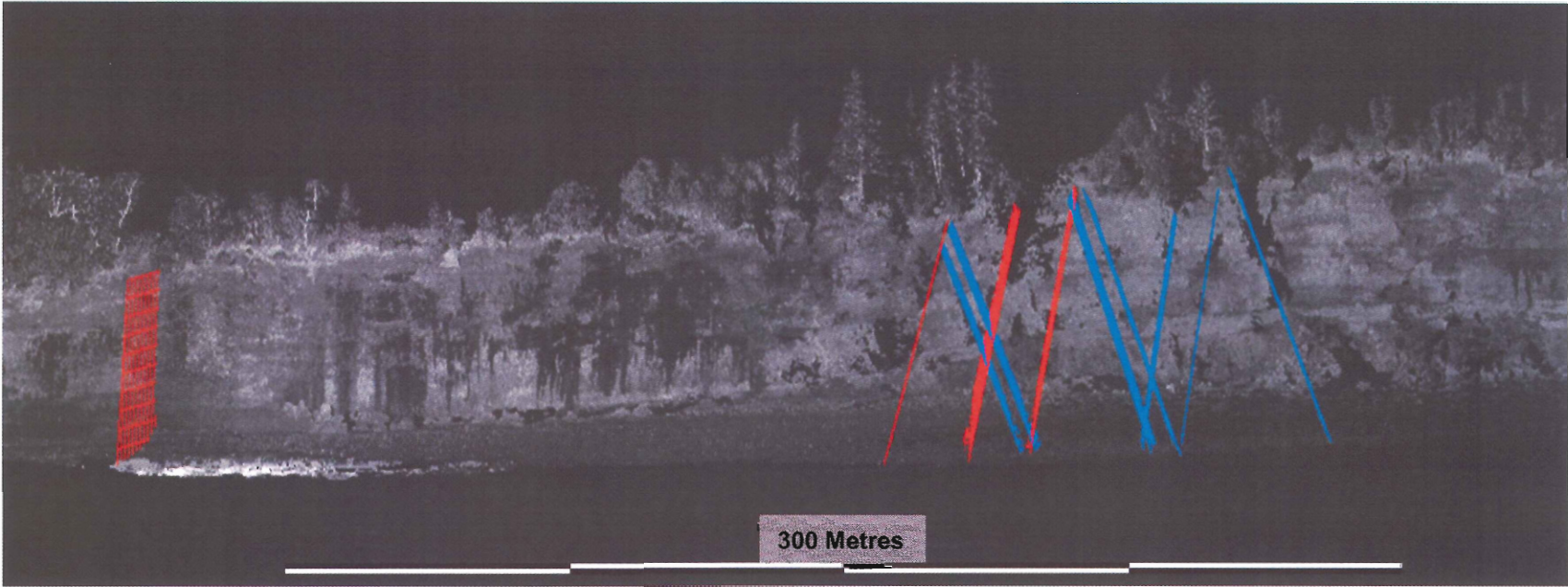


Figure 4.30: LiDAR image with all major faults red) and minor faults (blue).

5.0 Depositional Model

The data compiled from the outcrop study and the literature review of similar studies conducted on nearby Wolfville Formation outcrops, can be used to construct a depositional model of the lower 20 m of the Wolfville Formation.

Work conducted by Leleu et al. (2009) at Rainy Cove, 2 km west of Cambridge Cove, addresses the Wolfville Formation. This paper describes the Wolfville Formation from the Carboniferous-Triassic angular unconformity and subdivides the recorded 115 m thickness of the Wolfville Formation into several depositional environments. The lower 5 m of the formation has been described as an alluvial fan depositional environment, dominated by debris flows. The alluvial fan and debris flows grade into a fluvial braid channel environment. Hubert and Forlenza (1988) and Van Lanen et al. (2009) proposed similar conclusions east of Rainy Cove.

Good correlation exists between published Rainy Cove data (Hubert and Forlenza, 1988, Leleu et al., 2009; Van Lanen et al., 2009) and the results gathered from this study at Cambridge Cove. Stratigraphic work conducted at Cambridge Cove displayed architectural elements with low thickness, which are laterally extensive and capped by thin beds of medium- to coarse-grained sandstones, which include thin horizons of paleosols.

Further evidence that the lower 20 m of Wolfville Formation was deposited in an alluvial fan environment grading into a braided river depositional environment is provided by Gibling (2006) in his literature review of fluvial systems. Results compiled from the measurements of the large-scale sedimentary structures at Cambridge Cove have been averaged and plotted on a diagram (Fig. 5.1) modified from Gibling (2006).

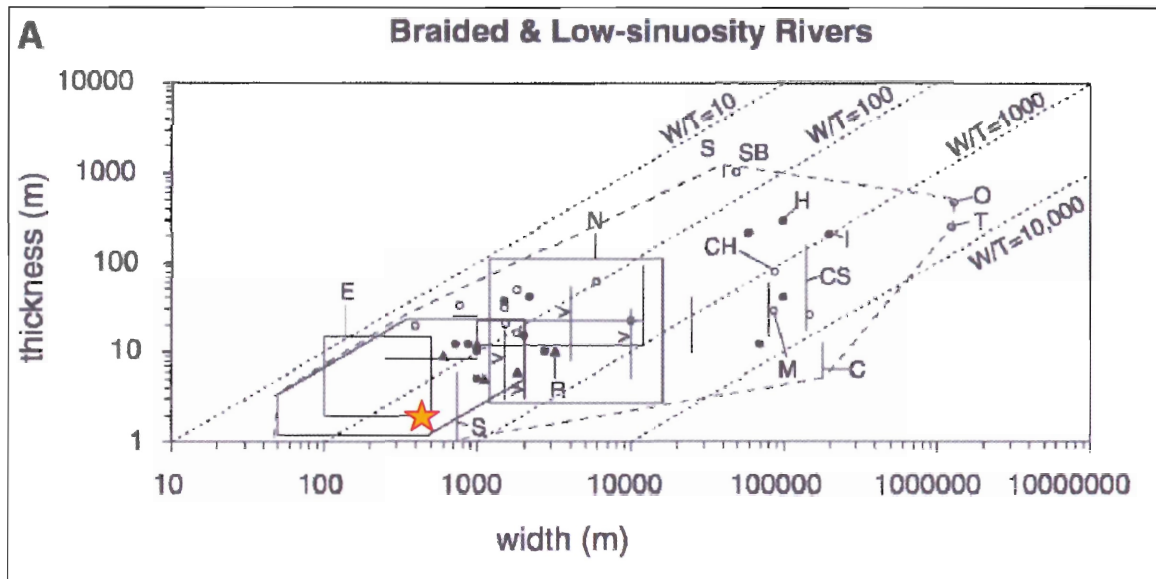


Figure 5.1: W/T plot for mobile Channel Belts; braided & low-sinuosity rivers. Cambridge Cove results plotted as red star (modified from Gibling, 2006).

The Cambridge Cove results plot close to results from studies of the Siwalik Group braided river deposit. The Siwalik Group, along with other deposits, is discussed in Gibling (2006) as:

"A group of very large channel bodies is prominent with widths greater than 40 km, thicknesses up to 1200 m, and areas of tens of thousands of square kilometers. These composite bodies are composed of many smaller, erosionally based bodies that are laterally and vertically stacked and comprise barform deposits and bedload sheets, as in the Castlegate Sandstone of Utah. Channel sedimentation is dominated by vertical accretion, and evidence for systematic lateral accretion and channel migration—although present locally—is uncommon. Fine-grained lenses within the bodies represent abandoned channel fills and floodplain remnants."

Figure 5.2 is a model by Hubert and Forlenza (1988), which depicts the deposition of sediments originating from the highlands of the pre-Triassic rocks into the newly formed Minas Basin.

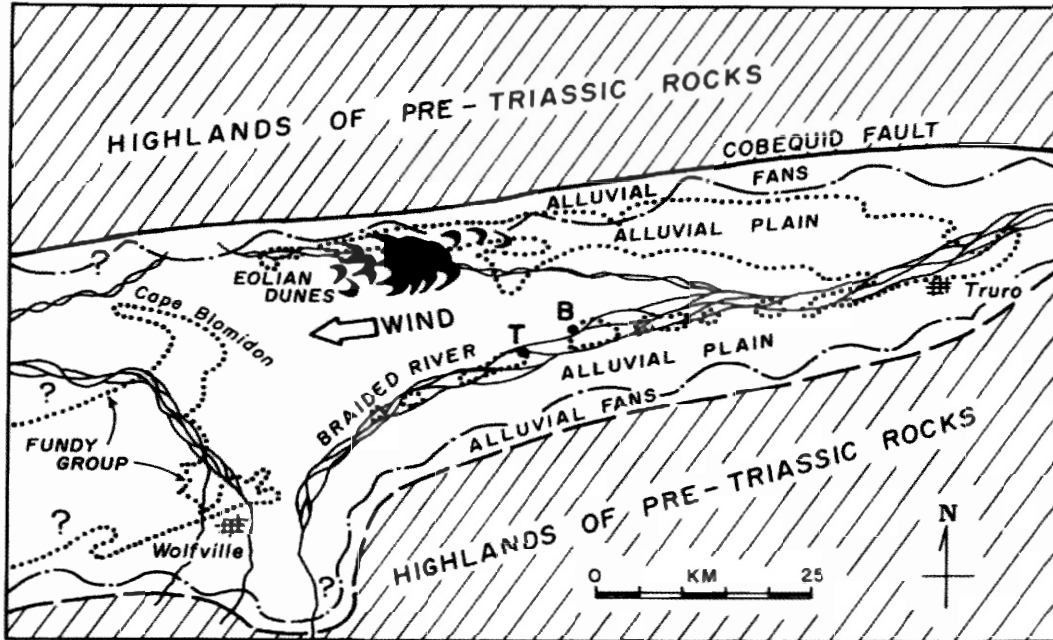


Figure 5.2: Depositional model of Wolfville Formation in the late Triassic (Hubert and Forlenza, 1988).

6.0 Discussion

Section 5.0 establishes that the depositional environment of the Wolfville Formation represents an alluvial fan environment grading into a braided river. This depositional environment comprises thin multi-channel bodies that have been subsequently infilled with laterally continuous beds comprising lithofacies 1- 4.

6.1 Permeability and Fluid Flow

Stratigraphic sections measured across the outcrop established that the lower 20 m of the Wolfville Formation contains four lithofacies: clast-supported conglomerates, matrix-supported conglomerates, medium- to coarse-grained sandstones and paleosols. Each lithofacies has a different permeability value determined by its lithology and diagenesis which controls the rate at which fluid can pass through the lithofacies. The greatest permeability is found in the clast-supported conglomerate (lithofacies 1), which features large clast sizes and minimal reduction of pore spaces from matrix filling. Hand samples of lithofacies 1 support this observation. Clasts are cemented together with an high amount of calcite, which may be due to migration of meteoric waters into this lithofacies during paragenesis. Permeability of matrix-supported conglomerates (lithofacies 2) appears to be less than lithofacies 1 permeability. Pore spaces between clasts are filled with medium- to coarse-grained sandstone. Thus, permeability is relatively decreased. Permeability results have been obtained for the medium- to coarse-grained sandstones (lithofacies 3) and are shown in Table 4.1. The results vary from 70 mD at the top of the cliff section to 800 mD at the base of the measured section of the Wolfville Formation. It should be noted that the results gathered from this method may not correspond to the actual permeability behind the cliff face or in the subsurface,

as surface weathering has occurred along the face of the outcrop. Permeability values increase down the cliff face may be due to; 1) the influx of tidal waters against the cliff face which aid in dissolving calcite from the matrix; 2) groundwater flow, which is observed near the base of the cliff at the contact between the Wolfville Formation and the fine-grained sediments of the Horton Group, which may dissolve calcite from the matrix. Paleosols found at Cambridge Cove (lithofacies 4) are assumed to have the lowest permeability values. These paleosols are comprised of fine-grained sandstones and siltstones with some carbonaceous material. This assumption is further corroborated by the observation of groundwater seeping out of the cliff section at the top of paleosol horizons.

Using the depositional model, structural features, and permeability results, we can address the controls on fluid flow within this braid channel complex and identify the key factors in compartmentalization of fluids within this simulated subsurface reservoir.

6.2 Gamma Logs

One of the main purposes of outcrop analogue study is to develop an understanding of the structures associated with a depositional environment, and use this knowledge to help understand subsurface reservoirs that were deposited under similar environmental conditions. Information of subsurface reservoirs is contained within seismic images, as well as borehole information such as gamma logs. Outcrop gamma logs can be used to increase the knowledge of the subsurface depositional environment by comparing the outcrop gamma logs with the subsurface gamma logs.

The gamma log that was created at Cambridge Cove (Fig. 4.18) displays results that could be possibly viewed as a different depositional environment if a similar log was retrieved from a borehole in a subsurface reservoir. Figure 4.18 illustrates the gamma log that was created while collecting section 1 and demonstrates a gamma signature that is distinctive to the Cambridge Cove sediment. Typical gamma curves tend to shift to the right when a fine-grained layer is encountered. This is due to the increased concentration of fine-grained minerals that contain radioactive elements. A left shift occurs when the gamma rays encounter clean sands (no silts).. The readings at Cambridge Cove were, in some instances, the direct opposite. The gamma curve shifted right when encountering the highly permeable clast-supported conglomerates (lithofacies 1). These results are most likely due to the nature of the clasts found within lithofacies 1. A high percentage of clasts comprise metasediments, which are rich in fine-grained sediments. If a bore hole were to be drilled in a deposit of similar clast composition, one would most likely interpret these intervals as impermeable fine-grained layers that would be barriers to horizontal fluid flow within the reservoir. This interpretation would affect net pay calculations and increase the chance of operators abandoning a possible productive hydrocarbon reservoir.

6.3 Compartmentalization

Section 6.1 described the permeability of each lithofacies found within the study area, and identified that fluid flows readily within the clast supported conglomerates (lithofacies 1) but has poor flow within paleosols (lithofacies 4). The results obtained from the high resolution photogrammetry and LiDAR identified the lateral extent of these

lithofacies, and the internal lithofacies architecture. It was found that clast- and matrix-supported conglomerate lithofacies 1 & 2, respectively, dominate the outcrop section with laterally extensive beds in the order of >100 m in width. The geometry of these large scale bedforms suggests a mixed depositional history, which includes individual channel belt and multi-story channel belt as proposed by Leleu et al. (2009). Some beds contain preserved channels that have been infilled with clast-supported conglomerate, whereas the large bedforms are laterally continuous and most of the channel bodies were eroded away and infilled during surges in deposition of sediment (Fig. 6.1).

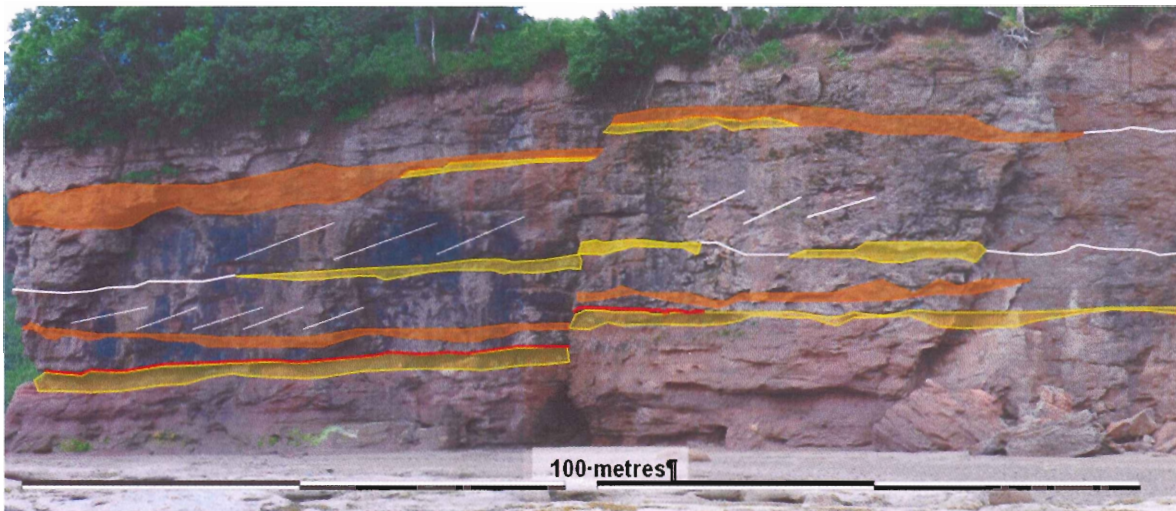


Figure 6.1: Multistory channel belts infilled by bar deposits (outlined in white) and some preserved channel bodies (orange).

Fluid within this type of reservoir would tend to migrate horizontally along the large scale barforms and occupy channel bodies due to; 1) the higher permeability of the conglomerates vs. the sandstones and paleosols and; 2) most of the cycles described at Cambridge Cove are capped by lower permeability lithofacies thus creating baffles and possible barriers for vertical fluid migration. This type of fluid flow creates

stratigraphic reservoir compartmentalization as the effective drainage of the reservoir is now diminished by creating pockets of fluid trapped within high permeable lithofacies, capped by baffles and barriers of low permeability lithofacies.

The structural features observed within the cliff face, add to the compartmentalization of the reservoir by offsetting stratigraphically connected bedforms and channel infills that comprise high permeability lithofacies. These structural features diminish the horizontal communication of the reservoir. As documented at Cambridge Cove, structural features can also increase the vertical fluid flow within the reservoir by creating vertical migration pathways. Fluids trapped within channel bodies and barforms can now migrate vertically and concentrate near the subsurface if an adequate seal is present. The major four faults described in Section 4.5.2 are assumed to be sealing faults, as they do not permit horizontal fluid flow and act as a horizontal fluid flow barrier. There are three lines of evidence to support this hypothesis: 1/ the high amount of calcite found within the fault, 2/the lack of water seeping out of the fault planes and 3/ the the migration of meteoric water vertically along the fault surface and sealing during diagenesis. The minor faults found within the outcrops provide both vertical fluid flow pathways and allowed horizontal communication between reservoirs due to the very low offsets.

7.0 Conclusions

Study of the exceptionally well preserved 2D and 3D outcrops at Cambridge Cove provides a detailed description of the stratigraphic features of the Wolfville Formation. From this study, four main lithofacies are identified: clast-supported conglomerate, matrix-supported conglomerate, medium- to coarse-grained sandstones, and paleosols. Architectural elements and structural features of the outcrop were identified by the construction of detailed sections, high resolution LiDAR scans in conjunction with high resolution photogrammetry. The use of these techniques also revealed the architectural identification of channel bodies and barforms. Using the data and background literature, a braided channel depositional model was established for the Wolfville Formation at Cambridge Cove.

Cambridge Cove can be used to develop an outcrop analogue for similar subsurface braid channel complexes. Permeability results from the lithofacies analysis provides insight into the nature of fluid flow within a simulated subsurface reservoir. Stratigraphic reservoir compartmentalization was investigated. It was concluded that fluid flow would tend to migrate laterally whereas vertical fluid flow was limited by reservoir baffles and barriers generated by highly permeable lithofacies, i.e.: clast-supported conglomerates which are capped by low permeability to impermeable lithofacies, i.e.: paleosol horizons. Two types of faults were identified and characterized in this study, sealing faults that act as baffles or barriers to flow, and transmissive faults that can allow lateral and vertical migration of fluids. Structural features found within the study area also played a key role in fluid migration by: 1) increasing reservoir compartmentalization by generating offsets of stratigraphically connected bedforms causing non-communication between the thick barforms and channel bodies, and 2)

increasing vertical fluid flow within the reservoir by creating vertical migration pathways along the fault surfaces.

8.0 References

- Baird, D., and Olsen, P.E., (1983) Late Triassic herptofauna from the Wolfville Fm. Of the Minas Basin (Fundy Basin), Nova Scotia, Canada (abstract): Geological Society of America, Abstracts within Program, v. 15, 122 p.
- Campbell, C.V., (1967) Lamina, laminaset, bed and bedset: *Sedimentology*, v. 8, p. 7-26.
- Fraser, J.A., (2010) Trends and architecture of Bluestone Formation turbidites in Point Pleasant Park, Halifax, Nova Scotia: Dalhousie University Department of Earth Sciences, Honours thesis, unpublished, p 1-81.
- Gibling, M.R., (2006) Width and thickness of fluvial channel bodies and valley fills in the geological record: a literature compilation and classification: *Journal of Sedimentary Research*, v. 76, p. 731–770.
- Google Earth., (2010). Satellite image of Nova Scotia. Google Inc. Accessed from <http://earth.google.com/>, March 15, 2010.
- Hodgetts, D., Drinkwater, N.J., Hodgson, D.M., Kavanagh, J., Flint, S., Keogh K.J., Howell, J., (2004) Three dimensional geological models from outcrop data using digital data collection techniques: an example from the Tanqua Karoo depocentre, South Africa. In Curtis, A. & Wood, R. (Eds.) *Geological Prior Knowledge*. Geological Society of London Special Publications, 239, 457-75.
- Hubert, J.F., and Forlenza, M.F., (1988) Sedimentology of braided-river deposits in Upper Triassic Wolfville redbeds, southern shore of Cobequid Bay, Nova Scotia: *Developments in Geotectonics*, v. 22, p. 231–237.
- Hubert, J.F., and Mertz, K.A. Jr., (1984) Eolian sandstones in Upper Triassic–Lower Jurassic red beds of the Fundy Basin, Nova Scotia: *Journal of Sedimentary Petrology*, v. 54, p. 798–810.
- Keppie, J.D., (1982) The Minas geofracture, in St. Julien, P., and Beland, J., eds., 4 Major structural zones and faults of the northern Appalachian: Geological Association of Canada Special Paper 24, p. 1-34.
- Klappa, C.F., 1980, Rhizoliths in terrestrial carbonates: classification, recognition, genesis and significance: *Sedimentology*, v. 27, p. 613–629.
- Leleu .S, Hartley A.J., and Williams B.P.J., (2009) Large-scale alluvial architecture and correlation in a Triassic pebbly braided river system, Lower Wolfville Formation (Fundy Basin, Nova Scotia, Canada): *Journal of Sedimentary Research* 79: 265–286.

- Makaske, A., (1998) Anastoming rivers - Forms, processes and sediments. Netherlands Geographical Studies p. 249-287.
- Miall, A.D., (1978b) Facies types and vertical profile models in braided river deposits: a summary, in Miall, A.D., ed., *Fluvial sedimentology: Canadian Society of Petroleum Geologists, Memoir 5*, p. 597-604.
- Miall, A.D., (1985) Architectural-element analysis: a new method of facies analysis applied to fluvial deposits: *Earth-Science Reviews*, v. 22, p. 261–308.
- Miall, A.D., (1991b) Hierarchies of architectural units in clastic rocks, and their relationship to sedimentation rate, in Miall, A.D., and Tyler, N., eds., *The three-dimensional facies architecture of terrigenous clastic sediments, and its implications for hydrocarbon discovery and recovery: Society of Economic Paleontologists and Mineralogists, Concepts in Sedimentology and Paleontology, V. 3*, p. 6-12.
- Miall, A.D., (1992) Alluvial Deposits Ch. 7 in, R.G. Walker and N.P. James, ed., *Facies Models-Response to Sea Level: Geological Association of Canada*, p 119-141.
- Monette, S., (2008), Cambridge Cove area LiDAR DEM/DSM generation and modern and Triassic Bar Investigation: Dalhousie University and Shell Canada (SELF) recognition plan, Unpublished.
- Olsen, P.E., (1990) Tectonic, climatic, and biotic modulation of lacustrine ecosystems-examples from Newark Supergroup of Eastern North America: in Katz, B., eds., *Lacustrine Basin Exploration: Case Studies and Modern Analogs, American Association Petroleum Geologists Memoir 50*, p. 209-224.
- Olsen, P.E., Schlische, R.W., and Gore, P.J.W eds., (1989) Tectonic, depositional, and paleoecological history of Early Mesozoic rift basins, eastern North America: Washington, American Geophysical Union, International Geological Congress Field Trip T351, p. 174.
- Olsen, P.E., and Schlische, R.W.,(1990) Transtensional arm of the early Mesozoic Fundy rift basin; penecontemporaneous faulting and sedimentation: *Geology*, v. 18, p. 695–698.
- O'Reilly, G., (1982) Uranium in Nova Scotia: A background summary for the uranium Inquiry, Nova Scotia: Department of Mines and energy. Report 82-7.
- Van Lanen, X.M.T., Hodgetts, D., Redfern, J., and Fabuel-Perez, I., (2009) Application of digital outcrop models: two fluvial case studies from the Triassic Wolfville Formation., Canada and Oukaimeden sandstone Formation., Morocco: *Geological Journal*, v. 44, p. 742-760.

Wach G.D., (2009) EARTH 4156 course lecture notes. Dalhousie University, Halifax, N.S.

Wade, J.A., Brown, D.E., Traverse, A., and Fensome, R.A., (1996) The Triassic–Jurassic Fundy Basin, eastern Canada: Regional setting, stratigraphy and hydrocarbon potential: *Atlantic Geology*, v. 32, p. 189–231.